An ex vivo model of *Toxoplasma* recrudescence.

Amber L. Goerner[1+], Edward A. Vizcarra[2+], David D. Hong[1], Kristina V. Bergersen[2], Carmelo A. Alvarez[1], Michael A. Talavera[1], Emma H. Wilson[2], and Michael W. White[1&]

[1]Department of Internal Medicine, Division of Infectious Disease and International Medicine, Morsani College of Medicine, University of South Florida, Tampa, Florida, USA. [2]Division of Biomedical Sciences, School of Medicine, University of California, Riverside, Riverside, California, USA

Running title: *Toxoplasma* ex vivo recrudescence

Key Terms: Apicomplexa, *Toxoplasma gondii*, development, tissue cyst, latency, chronic toxoplasmosis

+co-first authors.

[&]Address correspondence to:

Michael W. White
Department of Internal Medicine
Division of Infectious Disease and International Medicine
University of South Florida
3720 Spectrum Blvd, Suite 304
Tampa, FL 33612
email: mwhite.usf@gmail.com
office 813-974-8411
Fax 813-974-0804

ABSTRACT

Efforts to develop therapies against *Toxoplasma* reactivation have been hampered by the lack of an in vitro model of bradyzoite recrudescence. To overcome this issue, we established a new ex vivo model of bradyzoite recrudescence using bradyzoites from an unadapted Type II ME49 strain isolated from murine brain tissue to infect human foreskin fibroblasts and neonatal murine astrocytes. Bradyzoite infection of both host cell types produced two sequential tachyzoite growth stages that appeared similar to previous sporozoite in vitro infections; a fast-growing stage was followed by spontaneous formation of a slower-growing stage. In astrocytes, but not in fibroblasts, there was evidence of second bradyzoite to bradyzoite recrudescent pathway that occurred simultaneously with the bradyzoite to tachyzoite pathway. Thus, the host cell environment strongly influenced the pathway of bradyzoite recrudescence. Infections of mice with either the fast-growing or slow-growing recrudescent tachyzoites showed progressive decreases in brain cyst formation that could be fully recovered using serial tissue cyst passage demonstrating the loss of developmental capacity was reversible. By contrast, poor tissue cyst formation of laboratory-adapted tachyzoites was not reversible by these approaches indicating developmental incompetence was permanent in these strains. In order to develop methods to distinguish strain developmental competency, we identified *Toxoplasma* genes highly expressed in ME49EW in vivo tissue cysts and developed a qPCR approach that differentiates immature from mature bradyzoites. In summary, the results presented describe a new ex vivo bradyzoite recrudescence model that fully captures the reported growth and developmental processes observed during toxoplasmosis reactivation in vivo opening the door to the further study of these important features of the *Toxoplasma* intermediate life cycle.

INTRODUCTION

Reactivation of the *Toxoplasma* tissue cyst is a significant health threat to people chronically infected with this parasite and is life-threatening to infected individuals that are or become immunocompromised. Individuals acquire their initial *Toxoplasma* infection by ingesting oocysts from environmental sources or tissue cysts from contaminated food products. Oocysts and tissue cysts are exposed to proteases in the

GI track that release the sporozoite and bradyzoite stages, respectively, to invade epithelial cells lining the gut. The time from localized infection to systemic escape is relatively short in mice. By 2 h post-oral oocyst infection, *Toxoplasma* parasites have infected the intestinal epithelium and by 8 h the infection could be detected in the mesenteric lymph nodes (1). Based on sensitive bioassay methods, the tissue cyst form can be detected in 6-7 days in the brain of mice orally infected with the oocyst stage (2). The short timeframe from initial infection to the establishment of chronic disease makes it difficult, if not impossible, to prevent *Toxoplasma* infection, which accounts for the wide spread distribution of this parasite. It is estimated that one third of human populations are infected with this pathogen (3). Healthy individuals are at low risk for clinical complications from toxoplasmosis, although 10-20% of immune competent adults and children are symptomatic for this disease (4). *Toxoplasma* is one of the most frequent causes of inflammation of the uvea layer of the eye (3) and in some cases these infections results in the loss of vision. Relapsing disease is common in the first two years following a primary lesion diagnosis, especially in elderly patients (5). Prior to the introduction of HAART-therapy, *Toxoplasma* caused frequent life-threatening encephalitis in AIDS patients, with reactivating disease thought to be the most common cause (3). Today, *Toxoplasma* infections of AIDS patients remain a significant clinical threat to large populations that have poor access to HIV therapies and this will remain so until there is a HIV cure and/or a therapy is found to eliminate the chronic tissue cyst stage.

Recrudescence of the *Toxoplasma* bradyzoite tissue cyst is central to reactivation of toxoplasmosis, which is a developmental process infrequently studied and poorly understood. Studies of immunosuppressed mice indicate that *Toxoplasma* reactivation preferentially occurs in the brain frontal and parietal cortex grey matter (6), which is composed of neuronal cell bodies, dendrites and unmyelinated axons, and astrocytes and oligodendrocytes. There were few reactivating lesions observed in the cerebellum indicating this region has few tissue cysts (6), which was confirmed by tissue cyst mapping in the infected murine brain (7). Attempts to define the parasite developmental process associated with recrudescence in immunosuppressed mouse models and in AIDS patients that have succumbed to toxoplasmosis have uncovered heterologous parasite development in foci of reactivation (8, 9). Many vacuoles of different sizes filled with parasites expressing tachyzoite and/or bradyzoite

markers are present simultaneously in these lesions. Consequently, the original cyst rupture could not be identified nor could the sequence of parasite developmental steps or host cell contributions be discerned (8, 9). These limited studies point to the challenges in studying *Toxoplasma* reactivation, which currently is limited to animal models. What is critically needed is an in vitro model of bradyzoite reactivation that could accelerate efforts to understand these processes at the cell and molecular level.

In this paper, we describe a new ex vivo model of *Toxoplasma* recrudescence. The crucial foundation of this model is the use of a robust cyst-forming strain that has never been adapted to cell culture. We define two distinct pathways of bradyzoite recrudescence that are host cell-dependent. In addition, we introduce new markers that are able to differentiate bradyzoites based on developmental maturity.

RESULTS

Adaptation to cell culture leads to loss of *Toxoplasma* developmental competency.

One of the major challenges in studying the tissue cyst stage responsible for chronic *Toxoplasma* infections has been the preservation of developmental competency in experimental models especially cell culture systems. The Type II ME49EW strain has been exclusively maintained by alternating passage through resistant and sensitive mouse strains in order to sustain high tissue cyst production (see Fig. S1 for maintenance practice). From an i.p. infection of 10 cysts, the native ME49EW strain consistently produced thousands of tissue cysts in multiple mouse strains (CBA/j mouse infection, Fig. 1). To demonstrate the problems associated with cell culture adaptation, we infected human foreskin fibroblasts (HFF) with ME49EW bradyzoites and after 6 attempts (~30 million total bradyzoites plated) an adapted parasite line emerged and was cloned (ME49EW1 strain). An infection of 10,000 ME49EW1 tachyzoites was well tolerated by CBA/j mice, however, the competency to produce tissue cysts in murine brain tissue was dramatically reduced (EW1 tachy-to-cyst, Fig. 1). The reduction of ME49EW cyst production could not be reversed by infections of mice with a standard 10 cyst (i.p.) dose of ME49EW1 tissue cysts recovered from the tachyzoite infected mice (EW1 cyst-to-cyst, Fig. 1) and B1 gene-analysis verified that low ME49EW1 cyst counts in brain were not the result of a change in *Toxoplasma* distribution in mouse tissues. The loss of developmental competency following forced

adaptation to HFF cell culture is not an isolated outcome (10). Infection of CBA/j mice with two common laboratory strains (10,000 tachyzoites, i.p.) used to study bradyzoite development in vitro (PruQ and ME49-Tir1) (11, 12), also produced far fewer tissue cysts in CBA/j mice as compared to native ME49EW parasites (30 day PI average brain cysts; PruQ=25 cysts, ME49-Tir1=150 cysts). Poor in vivo tissue cyst numbers for the PruQ strain have been reported by many laboratories, which was recently cataloged (13). Like the ME49EW1 strain, secondary infections with PruQ tissue cysts did not reverse poor cyst production in CBA/j mice (Fig. S2A). The PruQ strain was engineered to express GFP under the control of the bradyzoite-specific LDH2 promoter (12), and therefore, bradyzoites in these cysts can be distinguished from tachyzoites by their green fluorescence. Microscopic examination of live PruQ tissue cysts from 30 day CBA/j infected mice showed they were smaller and less densely packed (Fig. S2C) than ME49EW cysts, which are more similar in appearance to the CDC reference image for this stage (Fig. S2B). We also noticed that all PruQ cysts had major gaps in GFP fluorescence (LDH2-GFP image, Fig. S2C), and these gaps contained parasites as shown by live DNA co-staining with Hoechst dye. Parasite nuclei in the GFP fluorescent gaps were larger and brighter (Fig. S2C) indicating there is a mixture of replicating tachyzoites and bradyzoites in these cysts, which is a tissue cyst phenotype recently reported for another Type II strain (14). Unfortunately, there were too few PruQ cysts to extend the analysis to free bradyzoite populations. By comparison, ME49EW tissue cysts were larger at 30 day PI (Fig. S2C) and when stained with Hoechst dye the cysts showed a dense complement of parasites with uniformly smaller nuclei. Cell cycle analysis of purified ME49EW bradyzoites (Fig. S3A, B) determined they were all mature bradyzoites (no SAG1 expression) with >98% 1N genomic content (G1/G0) and no microscopic evidence of mitotic forms (Fig. S3B, no u-shaped or double nuclei per parasite or internal daughter buds). The nuclei in ME49EW dormant bradyzoites had an unusual extreme posterior location (Fig. S3B) likely due to the large number of amylopectin granules (see bradyzoite EM studies ref. 15) that displace the typical central location of nuclei in replicating tachyzoites (16). It is not clear the posterior location of dormant bradyzoite nuclei would be compatible with endodyogenic replication. Combined these results are consistent with a G1/G0 cell cycle status for ME49EW bradyzoites that is similar to Type III, VEG strain bradyzoites produced by sporozoite infections

of CD-1 mice (17). In the absence of a suitable laboratory strain to investigate bradyzoite recrudescence, we optimized ME49EW tissue cyst production in CBA/j mice to reliably produce 5-10,000 tissue cysts per mouse cortex (cerebellum contains <5% of total brain cysts) with yields of 1-2 million purified bradyzoites (30-60% recovery) per mouse (see Materials and Methods and Fig. S1 for details).

ME49EW bradyzoite infections initiate dynamic growth changes.

In order to establish an ex vivo model of bradyzoite recrudescence, we investigated the developmental pathway that unfolds in ME49EW bradyzoite infections of two principle host cells, HFF cells and primary mouse neonatal astrocytes. HFF is the most common host cell used to study *Toxoplasma* development in vitro and astrocytes, which are relatively easy to culture, are a major host cell that bradyzoites encounter during recrudescence in brain and eye tissue (5, 18). Initial ME49EW bradyzoite infections of HFF cells using standard tachyzoite culture conditions showed poor growth, which we reasoned might be due to the oxygen levels in cell culture as bradyzoites in mouse brain reside in a low oxygen environment (19). By lowering oxygen levels from 21% to 5% (see Fig. S4 for further details), we were able to establish more robust ME49EW parasite cultures in HFF cells. Lower oxygen levels did not harm HFF or astrocyte host cells nor did lower oxygen alter the growth of HFF-adapted parasite strains, and therefore, all ME49EW cell culture experiments were performed under 5% oxygen. We anticipated it would be necessary to pass ME49EW parasite cultures in order to fully catalog the cell biological changes during ME49EW bradyzoite recrudescence over 1-2 weeks. Therefore, we followed a similar approach used to successfully characterize *Toxoplasma* sporozoite-initiated development (20) that is diagrammed in Figure S5.

Purified bradyzoites from ME49EW tissue cysts readily invaded HFF cells and neonatal astrocytes and followed a similar course of growth in both host cells during the first week. At the end of the first 24 h in HFF or astrocytes (Day 1-populations) the majority of vacuoles contained single parasites resulting in relatively few parasite doublings during this growth period (Fig. 2A, top H&E images). Parasite replication quickly accelerated in the second 24 h period (Day 2-populations) with many vacuoles containing 16 or 32 parasites by the end of Day 2 (doublings increased >5 fold, Fig. 2A). We estimated that ME49EW parasites post-Day 1 were dividing at rates equivalent to the fastest growing

laboratory strains (e.g. 6-8 h doubling of RH tachyzoites). Parasites growing at these faster rates possessed a larger nucleus, invaded nearby host cells at high MOI and the plaques showed a relatively clear lysis zone with less cellular debris (Fig. 2B, RH-like spreading). We have designated this type of growth as "RH-like". ME49EW population growth at the end of Day 3 was >6-fold over the bradyzoite inoculum used in both host cell types (Fig. 2C) with the vast majority of doublings occurring during the 48 h period from Day 2 through Day 3. Parasites continued to grow at a rapid rate in the second monolayers (Day 5-populations, Fig. 2C). One week from the initial bradyzoite infection, parasites in either host cell type had spontaneously slowed as evident by smaller vacuoles sizes and lower doubling rates in the third 48 h growth period (Day 7-images, Fig. 2A). Spreading behavior was also changed particularly in HFF cells with plaque development similar to many slow-growing laboratory strains; far less multiple invasions of nearby cells, parasites with smaller nuclei (indicative of G1), and cellular debris in a less defined lysis zone (Fig. 2B, Pru-like spreading). We have designated this type of growth "Pru-like". Longer cell cycle times in *Toxoplasma* laboratory strains are the result of extended G1 periods (16), which can be estimated from centrosome patterns. ME49EW parasites possessing single (G1 phase) versus double (S and M/C phases) centrosomes were equal in RH-like populations and nearly 2:1 in Pru-like populations (Fig. S3C). Slower growth became the dominant phenotype of all ME49EW populations post-Day 7 (Fig. 2C) and we never observed Pru-like parasites ever revert to RH-like growth in HFF or astrocyte cell cultures. Beyond one week, ME49EW parasites in HFF cells suffered a continued productivity decline (Fig. 2C) and became difficult to sustain. Second week cultures of ME49EW parasites in primary astrocytes continued to grow at a rate half that of Day 2-3 parasites, however, production did not further decline in astrocytes through Day 14 (Fig. 2C).

To better understand the nature of ME49EW parasite growth in HFF and astrocytes, we assessed the extracellular viability of parasites produced by bradyzoite infections in each host cell type. Rapidly growing RH-like parasites from Day 2-populations in HFF cells or astrocytes were purified and resuspended in culture media. The extracellular parasites were sampled every 6 h over a 30 h period and inoculated into either HFF or astrocyte monolayers. Plaque formation was quantified 48 h later by IFA assay. Native ME49EW Day 2-parasites from either host cell type were less stable in media (Fig.

S6) with ~88% of the parasites dying by 6 h (2-3 h half-life). By contrast, the HFF-adapted RH strain showed the opposite phenotype; extracellular incubation for 24 h in media was required before ~90% of RH parasites died. We next examined whether extracellular sensitivity was a characteristic of native Type II strains by examining the stability of a low passage Type I strain, GT1, which was used to produce genetic crosses in cats (21). Similar to ME49EW parasites, GT1 tachyzoites were more sensitive to media incubation with ~95% of parasites lost by 12 h extracellular (Fig. S6). Taken together, these results are a caution that native *Toxoplasma* strains may have lower stability in culture media and must quickly enter host cells to survive, whereas some HFF-adapted strains have been selected for increased extracellular stability, which is related to stress resistance (22). For the ME49EW tachyzoites forming from bradyzoite recrudescence, RH-like parasites were better at re-invading neighboring host cells than the Pru-like parasites post-growth shift, especially in HFF monolayers (Fig. 2B).

Host cells influence bradyzoite recrudescence.

To understand the developmental changes associated with ME49EW bradyzoite recrudescence, we investigated the expression of two key surface antigens; SRS9 present on bradyzoites and the tachyzoite surface antigen SAG1 (Figs. 3-4 and S7). As shown above, native bradyzoites invading host cells were uniformly SRS9+/SAG1- (Fig. S3B) and this did not change for many hours after invasion (Fig. 3A). By the end of Day 1, most vacuoles in either host cell type had a single SRS9+/SAG1- parasite (70% in astrocytes and 60% in HFFs). Between Day 1 and Day 2 post-bradyzoite infection, SRS9+ expression began to decline as replication dominated and SAG1 expression increased with many vacuoles having equal expression of these antigens (astrocyte images, Fig. 3A; HFF images Fig. S7). The trend towards elevated SAG1 and low to absent SRS9 expression progressively became the dominant phenotype as seen in Day 3-population images (Fig. 3A, quantified in D), and especially Day 5-populations (Fig. 3A,B) that formed in either host cell type. For the first time in an in vitro model, we observed SRS9+ only bradyzoites replicating in the first astrocyte monolayer (≥ 2 parasites/vac, SRS9-only=15% of vacuoles, Fig. 3C with additional examples Fig. S6B). Bradyzoite replicating vacuoles grew slower than tachyzoite vacuoles (see Figs. 2A and 4B) progressing from an average vacuole size of 5.22 (tachyzoite vacuole=10) at day 2 post-bradyzoite inoculation to a vacuole size of 12 by day 3 (tachyzoite

vacuole=21), while also failing to turn on SAG1 expression. Bradyzoite only replicating vacuoles (SRS9+/SAG1-) were observed in Day 5-populations, although at lower frequencies. The majority of Day 5-vacuoles were either SRS9+/SAG1+ or SRS9-/SAG1+ with SAG1+ only parasites clearly dominant (Fig. 3A,B). SAG1+ only parasites continued to dominate populations in HFF cells and astrocytes even after the growth of parasites had spontaneously slowed. However, in astrocytes a minor fraction of vacuoles (4%) containing SRS9+ only parasites were detectable after the Day 7-growth shift (see Fig. 4A for examples). While it was not possible to rule out that bradyzoite to bradyzoite replication gave rise to the Day 7-SRS9+/SAG1- vacuoles, there were many $SRS9^{Hi}/SAG1^{low}$ vacuoles (>30%) in Day 7-astrocyte cultures suggesting it was more likely parasites had invaded as SAG1+ parasites and then during replication turned back on SRS9 expression as SAG1 declined (re-development of the tissue cyst). In HFF cells, rare vacuoles staining exclusively for SRS9+ were present beyond Day 1, however this minor fraction of vacuoles contained single parasites. It is not known if these were nonreplicating bradyzoites being carried over or parasites that did not grow after passage and then re-expressed SRS9, while turning off SAG1. There was no clear evidence in the infected HFF cultures of any replicating bradyzoites.

We next investigated the formation of tissue cysts during ME49EW recrudescence using antibodies against the cyst wall protein, CST1 (Fig. 4B). In all HFF cell IFA analysis, CST1 expression was rare and <1% of the ME49EW vacuoles in HFF cells showed CST1 assembly into a cyst wall. Yet, Day 2-populations in HFF cells were >60% SRS9+, demonstrating that cyst wall formation and SRS9 expression do not always coincide. By contrast, in astrocytes spontaneous CST1 expression and incorporation into a cyst wall occurred in ~15% of vacuoles in Day 2-populations, which decreased to ~5% in Day 5-populations (Fig. 4B). The decrease in cyst wall formation in Day 5-populations was consistent with the growth dominance of the SRS9-/SAG1+ parasites at this timepoint in astrocytes. Following the shift to slower growth, spontaneous formation of cyst walls increased steadily through the end of the second week in astrocyte cell culture, although the fraction of vacuoles containing cyst walls never exceeded 20%. The level of cyst formation in astrocyte cultures exceeded the number of vacuoles observed undergoing bradyzoite-to-bradyzoite replication. Taken together, these results demonstrate

that ME49EW parasites are developmentally flexible and in the right host cell they are capable of re-developing tissue cysts at any time during recrudescence.

Defining new markers of mature bradyzoites.

It is clear that strains capable of robust in vivo cyst formation, such as ME49EW, are developmentally distinct from many HFF-adapted strains, although there are currently no molecular markers to distinguish these parasite strains. To identify new markers for the developmental competent ME49EW bradyzoite, we analyzed the transcriptome of ME49EW tissue cysts by RNA-sequencing (RNA-seq) and compared this data to other in vitro and in vivo bradyzoite mRNA datasets (Fig. 5 and Dataset S1). Two independent samples of ME49EW tissue cysts were purified from mice that had been infected with 10 cysts i.p. and harvested at 40 day PI. Tissue cysts were lysed, RNA purified and RNA-libraries prepared and sequenced as described in Materials and Methods. Illumina sequencing of the two ME49EW cyst RNA-libraries yielded >50 million reads with 13.8% aligned to the *Toxoplasma* reference genome. We analyzed ME49EW tissue cyst RNA-seq data in comparison to the in vitro ME49 tachyzoite RNA-seq data available from ToxoDB. Using a ≥2 fold cutoff, 4,340 mRNAs were differentially expressed in ME49EW cysts as compared to ME49 tachyzoites; 960 mRNAs were upregulated, 3,380 mRNAs were downregulated (Fig. 5A and Dataset S1). The ME49EW tissue cyst transcriptome was also compared to the transcriptome of ME49 tachyzoites induced to differentiate in alkaline-media (pH8.2) also available as RNA-seq data from ToxoDB (see Dataset S1 and Materials and Methods). Among the key gene expression differences between ME49EW tissue cysts and pH8.2-induced ME49 tachyzoites was the significant downregulation of many growth-related mRNAs (Dataset S1). Multiple DNA and RNA polymerases and DNA replication cofactors, 14 IMC proteins including IMC3 (14) that are needed for budding, mitotic factors such as centrin, as well as the classic S phase cell cycle marker DHFR-TS (25 fold down) are all significantly downregulated in ME49EW tissue cysts. This transcriptional profile is consistent with a dormant/G1/G0 state for the bradyzoites in these cysts as shown earlier (Figs. S2 and S3).

A list of some of the highest expressed mRNAs in ME49EW cysts that do not change or show lower levels of increase in pH8.2-induced ME49 parasites are shown (Fig. 5A red numbers, 5B-table)

and compared to another transcriptome analysis of in vivo tissue cysts (28 day cysts, Fig. 5B)(23). Utilizing the ME49EW cyst marker, TGME49_220560 (Fig. 5B, unknown protein), we developed a qPCR approach in order to follow the expression of a mature bradyzoite marker mRNA in the ex vivo bradyzoite recrudescence model. The features of this assay included primer sets for the tachyzoite marker SAG1, early bradyzoite marker SRS9, and actin depolymerizing factor as an internal reference gene. Each primer set passed standard quality control tests for use in qPCR. Total RNA was purified from ME49EW cysts and infected HFF monolayers of Day 1-, Day 2-, and Day 7-ME49EW recrudescent populations, and RNA was also purified from PruQ tachyzoites grown in normal pH 7.2 media or induced to differential in pH8.2 media (48 h, bradyzoites). Total RNA was converted to cDNA and used as template for SYBR-green qPCR analysis (see Dataset S1 for primers). A comparison of gene expression in these RNA sources defined two states of bradyzoite differentiation (Fig. 5C). A pattern of increased early bradyzoite marker (SRS9), continued SAG1 expression and the absence of TGME49_220560 expression indicated a state of bradyzoite immaturity, which was characteristic of the alkaline-media induced PruQ parasites and also ME49EW Day 2-recrudescing parasite RNA samples. By contrast, high levels of SRS9 and TGME49_220560 gene expression and the absence of SAG1 mRNA in ME49EW cyst RNA was consistent with bradyzoite maturity. The post-growth shift Day 7-recrudescent populations revealed an intermediate pattern between the immature PruQ pH8.2-parasites and the ME49EW in vivo tissue cyst bradyzoites with 25-fold increase in the expression of TGME49_220560 mRNA , while also expressing SAG1 mRNA.

Bradyzoites and recrudescing populations have distinct capacities to form tissue cysts in mice. We determined the cyst-forming capability of ME49EW bradyzoites, RH-like and Pru-like populations in CBA/j mice. Bradyzoites were obtained by excystation of purified ME49EW tissue cysts, while RH-like parasites were purified from bradyzoite-infected HFF or astrocytes at Day 3 PI. Pru-like parasites were from Day 7 growth-shifted populations as described in Figure S5. For parasites grown in HFF cells, three groups of ten CBA/j mice were infected with a dose of 10,000 parasites i.p. and tissue cysts were quantified in groups of five mice at 14 and 30 days PI (Fig. 6A). For parasites grown in astrocytes, three groups of 5 CBA mice were infected as indicated. Purified bradyzoites (Fig. 6A, closed circles) produced

the highest number of brain cysts indicating intact cysts are not required to achieve robust cysts numbers in mouse brain. RH-like parasites (closed squares) also produced reasonable cyst numbers, although not as high as the paired bradyzoite infections and RH-like parasites from astrocytes appeared to produce higher cyst counts. Regardless of the host cell used, infections with Pru-like parasites resulted in significantly lower cyst numbers in CBA/j brain tissue. To evaluate whether alterations in tissue distributions might explain the difference in brain cyst counts, we performed B1 gene analysis on other tissues from the 14 and 30 day mice infected with HFF-derived parasites (Fig. 7). Relative parasite burden in the brain of these mice correlated well with the cyst count data. At days 14 and 30 PI, bradyzoite infections showed the highest B1 gene signals in brain tissue with Day 3- and Day 7-parasites having stepwise lower burdens (Fig. 7A). Other tissues had detectable B1 gene levels that were a fraction of the levels in brain indicating that changes in tissue distribution could not explain the cyst count differences. The preference of *Toxoplasma* encystment in brain appears to be a unique characteristic of mice and other rodents (1). Because cytokine response is related to parasite burden, we collected blood at various times in the mice scheduled for tissue cyst counts at Day 14 PI and quantified IFNγ levels (Fig. 8). Peak IFNγ levels at seven days post-infection with bradyzoites and RH-like parasites follows a timing that has been previously reported (24), while the delay in peak IFNγ levels in mice infected with Pru-like parasites was consistent with the significantly lower parasite burden in mice infected with these parasites (Fig. 7B).

We next determined whether low cyst formation of Pru-like parasites was permanently compromised. Three groups of five mice were infected with 10 cysts from the first round of infections and cysts numbers from these secondary infections were determined at 30 days PI. Secondary cyst counts were significant and equivalent in these mice irrespective of the source of the original parasite infection (Fig. 7B) indicating that any loss of developmental competency in ME49EW recrudescence populations was fully reversible.

To further understand how bradyzoite-initiated recrudescence contributes to tissue cyst formation, we infected CBA/j mice with native ME49EW bradyzoites and then blocked parasite growth by adding sulfamerazine to drinking water at various times (Fig. 9, top diagram). Groups of five mice were infected

with 10,000 bradyzoites and subjected to sulfamerazine treatment for a period of ten days starting three days PI and continuing until day 12 PI. At 30 days PI, the brain cyst numbers were determined. The addition of sulfamerazine to drinking water at Day 3 PI effectively reduced tissue cyst numbers by >400 fold over no drug controls, while addition at Day 9 PI reduced average cyst numbers 13 fold. Treatment started at 12 days PI had no significant effect on average cyst numbers in 30 day infected mice. These results were consistent with the finding that bradyzoites and RH-like populations that formed early in bradyzoite recrudescence have the greatest capacity to produce brain tissue cysts in CBA/j mice (Fig. 6).

DISCUSSION

Why some *Toxoplasma* strains produce thousands of tissue cysts in mouse brain, while other strains produce a couple dozen is not understood. The Type II strains, ME49EW and PruQ studied here appear to be largely equivalent in the alkaline-stressed in vitro model; both strains slow growth in pH8.2 media, and robustly assemble cyst walls in 48-72 h cell cultures. Yet, these strains differ by two orders of magnitude in the ability to produce tissue cysts in mice (Fig. S2A). The limitations of the cyst wall as a functional developmental marker was recognized nearly 30 years ago (25) and even more recently (26). In a classic example, Type I, GT1 tissue cysts (cyst walls verified by TEM) from 6 day, but not earlier monocyte cultures were infectious for cats and produced oocysts in a short prepatent time, which is a feature of mature bradyzoites (25). Our examination of 30 day PruQ brain cysts in this study revealed much greater tachyzoite and active growing characteristics than 30 day ME49EW cysts, and thus, even after a month post-infection PruQ tissue cysts were still immature. By comparison, multiple independent criteria demonstrated that ME49EW tissue cysts were filled with mature, dormant bradyzoites. ME49EW bradyzoites do not express SAG1 protein or mRNA and have a uniform 1N genomic DNA content similar to Type III, VEG bradyzoites (17). In addition, we were unable to detect any evidence for mitotic parasites in ME49EW bradyzoite populations as was recently reported (14) and the ME49EW tissue cyst transcriptome (prior to excystation) indicates bradyzoites inside these cysts are deeply growth-arrested (G0 state). A simple conclusion is that the degree of bradyzoite maturity, not the presence of a cyst wall, explains the large difference in ME49EW versus PruQ cyst productivity in mice, or alternatively, cysts

with mixtures of tachyzoites and bradyzoites may be less productive. In healthy mice, infections with immature tissue cysts might prime the immune system against tachyzoites and bradyzoites leading to lower parasite burdens and cyst formation. The first hint that cross stage immunity would reduce cyst numbers came from expressing SRS9 in a tachyzoite (27), and we believe multistage immunity also explains why AP2IV-4 (transcriptional repressor) and protein kinase A knockout transgenic strains, which readily form immature cysts in alkaline cell culture, produce few to no cysts in mice (28, 29).

In these studies, we were able to convert the robust cyst-forming ME49EW strain to a poor cyst former through forced adaption to grow in HFF cell culture. The ME49EW1 line did not emerge easily as it required six separate platings of bradyzoites in HFF cells (~30 million bradyzoite inoculations total) to overcome the propensity of these cultures to die out (harvest < inoculum). These results suggested the worrisome idea that HFF-adapted ME49EW1 parasites arose due to genetic mutation; an idea that was reinforced by a small mutagenesis experiment (Alvarez and White, personal communication). Using mutagenesis conditions that generated temperature sensitive *Toxoplasma* mutants (30), we exposed ME49EW bradyzoite-infected HFF cultures to ethyl nitrosourea, which led to the emergence of multiple HFF-adapted parasite lines from a single bradyzoite plating (2 million bradyzoites). It is well known that repeated passage in HFF cells exacerbates the loss of developmental competency (reviewed in refs. 10, 31), therefore, even if developmental competency is only partially affected after the initial HFF-adaptation, it is likely to be fully lost over time in HFF cell cultures. Taken together, these results indicate there is an underlying genetic basis that causes developmental losses to become permanent in many strains like PruQ and ME49EW1, whereas, the temporary loss of developmental competency of the ME49EW "Pru-like" recrudescent population is likely due to epigenetic changes that are fully reversible. We do not understand the molecular basis for the permanent loss of developmental competency of lab strains and we also lack molecular markers that distinguish the developmental endpoints of in vitro versus in vivo cysts. The mature bradyzoite mRNAs we have identified and investigated in this study could provide new markers to optimize in vitro models and eliminate strains that are developmentally incompetent.

The poor developmental outcomes that result from adapting native ME49EW parasites to HFF cell culture raises the question of what are the parasites losing? The studies here of ME49EW bradyzoite recrudescence suggest some answers. Native ME49EW bradyzoite-infected cell cultures produced two basic types of SAG1+ tachyzoites in sequential order that are similar to the fast-growing followed by slow-growing tachyzoites that emerge from sporozoite infections (20). It is remarkable that native bradyzoites and sporozoites follow the same developmental pathway in the intermediate host. Importantly, the sequential steps in this developmental pathway appear to be critical to achieve high cyst numbers in mouse brain tissue. Through direct infections of mice with selected recrudescent populations and sulfamerazine-blocking experiments, we determined that infections of animals with ME49EW bradyzoites produced high cyst numbers, while blocking early following bradyzoite infections but not later caused tissue cyst numbers to plummet to zero in many mice. Infecting only with "RH-like" tachyzoites, and especially with growth-shifted "Pru-like" tachyzoites, lowered tissue cyst numbers. For the "Pru-like" parasite infections the very low parasite burden indicates that most of these parasites are eliminated before they can reach suitable tissues to form cysts, although these parasites might have the greatest cyst-forming potential. These results indicate the complete ME49EW recrudescence pathway that unfolds over one week following bradyzoite infections is required for expansion, dissemination, and establishing tissue cysts in brain tissue and this is consistent with a recent study showing maximum tissue cyst formation in pig muscle is reached seven days after oral infection with tissue cysts from mice tissues (32). Laboratory-adapted strains are unable to reproduce many of the key features of this bradyzoite recrudescence pathway. When *Toxoplasma* is adapted to cell culture, a number of interrelated characteristics change. HFF-adapted tachyzoites show 1) changes in the cell cycle, which becomes permanently faster due to a shorter G1 phase as passage number rises, 2) extracellular viability increases, 3) developmental competency decreases, and 4) virulence in mice also increases. The dilemma for the field is to decide when HFF-adapted strains are a suitable choice for developmental study and when they are not. The large genetic toolkit now developed with HFF-adapted strains is advancing our understanding of *Toxoplasma* biology at an ever faster pace. Based on the model work

described here, we are confident this genetic toolkit can be adapted to work with native bradyzoites that will permit genetic manipulation, while preserving developmental competency.

The best in vitro models reproduce the full breadth of natural processes. The relatively few studies of bradyzoite recrudescence in mice and humans have uncovered evidence that bradyzoite recrudescence is nonsynchronous (8, 9) resulting in actively replicating tachyzoites and all stages of bradyzoite re-development from immature to mature cysts being present in the same lesion (8). In addition, there is some indirect evidence in vivo bradyzoites can replicate without differentiating into tachyzoites (33). The ex vivo model of bradyzoite recrudescence presented here captures all these features with greater cell biologic and temporal resolution. The rapid differentiation of ME49EW bradyzoites into a fast-replicating tachyzoite tracked with the same timeframe in both HFF and astrocytes as did the shift to slower growth indicating the growth changes are likely host cell-independent. The opposite was true for developmental changes, which were strongly influenced by the host cell environment consistent with studies of *Toxoplasma* infections in muscle cells (34). The astrocyte environment was more permissive for ME49EW bradyzoite development than HFF cells with spontaneous formation of developmental stages that we don't see using laboratory strains and HFF cells. Following bradyzoite infection of astrocytes, 15% of the vacuoles were undergoing bradyzoite to bradyzoite replication and these vacuoles grew much slower than the tachyzoite vacuoles also forming in astrocyte cultures. These results indicate there are two distinct bradyzoite recrudescence pathways unfolding in astrocytes, while HFF cells only support the bradyzoite to tachyzoite pathway. Bradyzoite replication may permit *Toxoplasma* to expand and maintain tissue cysts without eliciting an immune reaction. Thus, ME49EW-infected astrocyte cultures at Day 2-3 are representative of the heterologous milieu of *Toxoplasma* developmental stages observed in brain lesions of individuals suffering AIDS and immunosuppressed mice (8, 9). Developmental heterogeneity was reduced as the dominant tachyzoite population took over HFF and astrocyte cultures, which is likely a progression that mimics the parasite expansion associated with fatal *Toxoplasma* encephalitis. The post-growth shift cultures also demonstrated developmental differences. In astrocytes, but not HFF cells, we observed increased re-development of the SRS9+/SAG1- bradyzoite through a mechanism of gene expression switching rather

than bradyzoite replication. The remarkable spontaneous shift to slow growth in recrudescing populations, which was also observed in IFNγ-knockout mice in sporozoite studies (20), likely occurs during bradyzoite recrudescence in vivo, although it would be difficult to see this timing in the chaotic landscape of a reactivated necrotic lesion. The ME49EW ex vivo recrudescence model solves that problem. It is often assumed that *Toxoplasma* developmental progression primarily occurs in response to immune stress. The results here indicate the spontaneous growth and developmental changes in ME49EW-infected astrocytes are the result of parasite-encoded mechanisms responding to signals from the host intracellular environment. There are no immune cells or cytokines added to these cultures. Encystation of *Toxoplasma* in mice occurs preferentially in neurons (35, 36), and this too is also parasite-encoded. In experiments with developmentally competent strains, cysts form in cultured neurons in normal media at the levels only achieved in HFF cells by stressing the cultures with alkaline-media (Bergersen and Wilson, personal communication). Thus, the alkaline-stress equivalent in animals is the neuron cell environment and other cells that provide similar signals such as mature muscle cells. There is evidence that a regulatory network that prevents host cells from growing is sufficient to promote bradyzoite development of some parasite strains (34). The mammalian nuclear factor CDA.1, which is highly expressed in brain tissue, and the cell cycle inhibitor $p21^{Wafi/Cip1}$ are components of this anti-growth network (34). Overexpression of CDA.1 imparts a bradyzoite-promoting effect on host cells without the need for stress or drug induction (37). The molecular basis for how the developmental program of *Toxoplasma* senses the post-mitotic environment of neurons and muscle cells is not known and an important area for future studies.

In summary, the dormant bradyzoite in ME49EW tissue cysts possesses remarkable developmental flexibility and ability to tailor the parasite-encoded developmental program to the type of host cell infected, which is fully captured in a new ex vivo astrocyte recrudescence model. In the right host cell, ME49EW parasites can chose to replicate as bradyzoites or fully convert to the tachyzoite stage in order to disseminate. Native bradyzoites, like the sporozoite stage, develop into the tachyzoite stage using a two-step pathway that permits rapid biomass expansion but is also self-limiting. These versatile tachyzoites also have the ability to re-develop into the dormant bradyzoite at any time within a

host cell environment that is permissive for tissue cyst development. Adapting native strains to HFF-culture can disrupt these pathways and may cause transcriptional confusion as recent single parasite RNA-seq studies have suggested (38).

MATERIALS AND METHODS

Parasite strains and host cells.

All laboratory-adapted strains were maintained in human foreskin fibroblasts (HFF) cells in high glucose DMEM with sodium bicarbonate (Sigma) supplemented with 5% heat-inactivated fetal bovine serum (FBS) and 1% penicillin-streptomycin in humidified incubators at 37C with 5% CO2. The Type II ME49EW strain (kindly provided by Emma Wilson, U. California Riverside) was exclusively maintained in mice as described in Figure S1 and below. The strain ME49EW1 was obtained by forced adaptation of the parent ME49EW strain to grow in HFF cells and then cloned by limiting dilution. ME49EW1 grew well in HFF cells in the standard tachyzoite conditions described above including ambient air oxygen levels (21%). Several other HFF-adapted laboratory strains were used in this study: RH (Type I RH Δ*hxgprt*)(39), GT1 (low passage Type 1 strain)(40), PruQ (Type II Prugniaud Δ*ku80*, Δ*hxgprt::*LDH2-GFP)(12), and ME49-Tir1 (Type II ME49-Tir1-3 Flag)(11).

Astrocyte purification. Neonatal C57Bl/6 mice born at 0-3 days were sacrificed via decapitation and brains (without cerebellum) dissected and placed in cold wash media (DMEM and 2% fetal bovine serum). Brains were pooled and homogenized through a sterile 40 micrometer cell strainer (Corning) using a 3 ml syringe plunger. Homogenate was washed twice with cold wash media and spun at 2,000 rpm for 10 minutes at 4°C. Homogenate was resuspended with 6 ml per brain of prewarmed complete media (DMEM [Corning]; 10% FBS; 1% Nonessential Amino Acids Mixture 100x, [Biowhittaker Reagents Lonza],1% GlutaMAX supplement 100x [Thermo Fisher Scientific], 1% penicillin-streptomycin, [Genclone], 1% HEPES Buffer solution 1M [Thermo Fisher Scientific]. Resuspended cells were plated in non-vented T-25 cm^2 flasks with loose caps at 37°C, 5% CO_2. At days 3, 5, and 7 astrocyte media was replaced. To remove contaminating less adherent microglia and oligodendrocytes, astrocytes were shaken on day 8-10 at 260 rpm, 37°C for 1.5 hours. Media was replaced and cultures were shaken for

an additional 24h at 100 rpm, 37°C. Astrocytes were lifted with 3ml of 0.25% Trypsin EDTA, counted, and plated at a density of $1x10^6$ cells per T-75cm^2 vented flask until confluent.

Animal experiments.

All animal research was conducted in accordance to the Animal Welfare Act. C57Bl/6, CBA/J, and SWR/J #689 mice obtained from Jackson Laboratory (Jackson ImmunoResearch Laboratories, Inc., West Grove, PA, USA) were bred and maintained in a pathogen free vivarium under the Institutional Animal Care and Use Committee (IACUC) protocols established at the University of California, Riverside and the University of South Florida.

The ME49EW strain was continually passed through 5 to 6 week old female mice by first infecting resistant strain SWR/J (Swiss Webster) with 10 cysts in 200μl of cortex homogenate by intraperitoneal (i.p.) injection (see Fig. S1 for details). Tissue cysts in brain homogenates from infected SWR/J mice were then used to infect CBA/J, sensitive mice (10 cysts in 200μl diluted brain homogenates, i.p.).

Brain homogenate preparation. At 14-60 days PI as indicated, infected SWR/J or CBA/J mice were euthanized, brain cortices dissected and placed in 3ml of cold PBS (cerebellum was discarded as it contained <5% of total brain tissue cysts). Tissue homogenization and tissue cyst yields were significantly improved (tissue numbers >50% higher) by storing infected brain cortices overnight at 4°C in PBS. In direct comparisons, we determined tissue cysts held in brain tissues for up to 24 h in cold PBS were viable, fully infectious, and yielded active excysted bradyzoites. After the 4°C overnight storage in 3ml of 1xPBS, cortexes were easily serially homogenized by 3-4 serial passes through 18, 20 and finally, 22 gauge (blunt) sterile needles. Tissue cyst quality and enumeration was determined by a full examination of 30μl (x 3) of homogenate spread on a microscope slide. All tissue cyst mouse inocula used in this study were diluted to 10 cysts in 200μl in 1xPBS. In addition, the quantification of brain tissue cyst counts in mice infected with various parasite sources followed these protocols and were determined in triplicate.

Tissue cyst purification and bradyzoite excystation. Cysts were purified from mouse brain cortices infected with the indicated parasite numbers/cysts for 30-50 days. To purify tissue cysts, brain cortices were harvested and homogenates prepared as above (one cortex per 15 ml conical tube as combining

cortices reduces cyst yields). Following cyst counts as above, homogenate volumes were brought up to 11ml with PBS, mixed by inversion, and then centrifuged at 500xg for 15 minutes. The supernatant was removed by aspiration and the homogenate pellet resuspended in 2.5ml of percoll-90 (90% percoll, 10% 1xPBS) followed by the addition of PBS to a final volume of 7.5ml (final percoll=30%). The tube was fully mixed by several inversions and then centrifuged at 1000xg for 15 minutes without a brake. Tissue cysts pelleted in this gradient protocol, while debris collects at the top of the gradient, therefore, the supernatant was carefully removed by aspiration. If multiple cortices are used, the pellets containing tissue cysts were combined and the total volume raised to 10ml of PBS, followed by centrifugation at 30xg for 10 min and then removal of the supernatant by careful aspiration. The low speed 30g spin pellets medium to large tissue cysts (majority of bradyzoites) while retaining >80% of red blood cells in the supernatant. To obtain free bradyzoites, the tissue cysts were resuspended in excystation solution (5mg/ml pepsin, 100mg/ml NaCl, 0.14N HCl), incubated for 90 seconds and then 10 ml of culture media containing 5% fetal bovine serum added. Bradyzoites counts were obtained using a hemocytometer. A more detailed protocol with tips for successfully producing and purifying tissue cysts and free bradyzoites is available upon request.

Infections of mice with laboratory strains and recrudescing populations. ME49EW bradyzoites and parasites at various times during recrudescence in HFF or astrocyte cells, as well as laboratory strains grown in HFF cells, were purified from host cell monolayers by standard scrape, needle pass, and filter methods and diluted to 50,000 parasites/ml in PBS. We have determined experimentally that filtration of needle-passed parasite cultures through 3 micron filters removes >95% of trypan blue positive (dead) parasites. Groups of CBA/J mice as indicated were infected i.p. with 0.2ml of the appropriate inocula. Mouse infections were used to determine parasite burden, cytokine expression and tissue cyst formation.

Serum Cytokine ELISA. Serum was harvested from mice via tail vein bleeding on days 3, 5, 7, 9, & 14. Blood was centrifuged at 16,000 RPM for 20min. Serum was aliquoted and stored at 80°C. IFNγ capture antibody (ebioscience: 14-7313-81) was incubated overnight at 4°C [1:1000]. Recombinant IFNγ (ebioscience, cat#: 14-8311-63) was used to create the standard. Standard and serum samples were

incubated at 37°C for 2h. Biotin conjugated anti-mouse IFNγ (clone:R4-6A2; ebioscience13-7312-85) was incubated at 37C for 1h. Peroxidase conjugated streptavidin (Jackson immune research 016-030-084) was incubated for 30min at 37°C. TMB substrate (Thermo, N301) is used for the colorimetric reaction, and an equal part of 0.16M sulfuric acid was used to stop the reaction. Standard curve and analysis were done in GraphPad Prism (GraphPad Software).

Sulfamerazine treatment. CBA/j (25 mice total) mice were each inoculated with 10,000 excysted ME49EW bradyzoites by i.p. injection. At various times following infection (see Fig. 9 for details) sulfamerazine (444 mg/liter) (41) was added to the drinking water of selected groups of mice. At 30 days PI, mice were euthanized, brain cortices removed and tissue cysts in homogenates enumerated in triplicate.

Ex vivo bradyzoite recrudescence experiments

Preliminary investigations determined that native ME49EW parasites grew better in HFF cells under lower oxygen levels. Therefore, throughout this study we cultured ME49EW parasites in HFF or neonatal astrocyte monolayers that were placed in a hypoxic chamber and grown in the same media with the exception that astrocytes received a 1% GlutaMAX supplement (see Fig. S4 for further details). Confluent HFF or neonatal astrocyte monolayers were inoculated at various times with excysted bradyzoites, lab strains or recrudescing populations at a MOI ~0.5. ME49EW parasites were passaged into new monolayers of either host cell type using the schedules shown in Figure S5.

Growth rate doublings. Post-excysted bradyzoites and Day 3- and Day 5-recrudesing populations were inoculated onto 6 well coverslips of HFF or astrocyte cells and at various times were fixed and stained using an anti-toxoplasma antibody (abcam, ab138698). Vacuole sizes at each timepoint were determined by counting 50 random vacuoles in triplicate on a Zeiss Axiovert fluorescent microscope. For each coverslip, the average number of parasite doublings per day was determined from the raw vacuole sizes (vac of 2=1 doubling, vac of 4=2 doublings, vac of 8=3 doublings etc.) divided by the total days in each incubation period.

Visualization of parasite growth and development. ME49EW bradyzoites and various recrudescing populations were inoculated onto 6 well glass coverslips of HFF or astrocyte cells at 0.5

MOI. All coverslips were cultured under low oxygen conditions as described in Figure S4. Infected coverslips were fixed with 4% PFA for 10min. Cells were permeabilized with either 100% acetone or 0.25% Triton-X for 10min. Cells were blocked with either 5% donkey serum or 1% BSA for 30min, followed by a 1 h incubation of the following primary antibodies diluted in blocking buffer: rabbit-anti SRS9 [1:1000] and mouse-anti SAG1 [1:1000](kindly provided by John Boothroyd, Standford U.), rabbit-anti-Toxo [1:500] (Abcam), mouse-anti-CST-1 [1:1000](kindly provided by Louis Weiss, Albert Einstein COM), mouse-anti-IMC1[1:1000](kindly provided by Gary Ward, U. Vermont), rabbit-anti-centrin [1:500](used 2 hour primary incubation). Secondary antibody master mix were incubated for 1h: Goat-anti-rabbit-AF568 [1:1000], Goat-anti-mouse-AF488 [1:1000], DAPI (1mg/ml). All incubations were done at room temperature, and all washes used 1XPBS.

Extracellular viability. Day 2-recrudesing ME49EW parasites (bradyzoite infection of HFF or astrocytes) and RH and GT1 parasites were purified and resuspended in 37°C growth media without host cells. The host-free parasites (10,000/cover slip) were used to immediately inoculate cover slips of the host cell type they were obtained from, and then again, every 6 h through 30 h. Parasites were incubated at 37°C throughout the experiment and ME49EW parasites were cultured in hypoxic chambers, while lab-adapted strains (RH and GT1) were cultured under standard ambient oxygen conditions. After 30 h coverslips were left to grow undisturbed for 48 h prior to being fixed and IFA analysis performed using anti-toxo primary antibody. Microscopic quantification of parasite plaques was determined by counting the number of vacuoles per field for a total of 10 fields (in triplicate). Percent survival was determined in comparison to the time 0 infections.

Parasite burden.

Organ tissues (brain, lung, muscle, liver, heart) were harvested from mice 14 days or 30 days post infection, and stored at -80°C prior to DNA purification. DNA was purified using a DNeasy minikit (Qiagen) according to manufacturer protocols. The qPCR reaction volume used 600ng of DNA from each organ, 0.375μM B1 gene primers (Forward:5′- TCCCCTCTGCTGGCGAAAAGT-3′; Reverse: 5′-AGCGTTCGTGGTCAACTATCG-3′), and 2x Luna universal qPCR master mix (New England bio labs) in a 25μl total volume. The amplification program was: 3 min at 95°C, 40 cycles of 10s at 95°C for

denaturation, 30s at 60°C for annealing, followed by 5s at 65°C and 5s at 95°C for extension. The realtime data was collected on a CFX96 Real-Time system, C1000 Touch thermal cycler using Bio-Rad CFX maestro software. A standard curve was generate based on serial dilution of purified ME49 genomic DNA. All results were expressed as the pg of parasite genomic DNA calculated from an experimentally generated standard curve generated in each PCR run.

Gene expression.

RNA purification. Total RNA from ME49EW cysts and Day 1-, 2-, or 7-recrudescent populations as well as PruQ tachyzoites and alkaline-induced PruQ bradyzoites (pH8.2 media for 72 h) were purified using the RNeasay kit (Qiagen) according to manufacturer protocols. Two biological replicates were prepared for each RNA source and RNA quality was assessed using an Agilent 2100 Bioanalyzer (Waldbronn, Germany).

RNAseq analyses. ME49EW tissue cyst RNA samples prior to excystation were processed for RNA-sequencing using the NuGen Universal RNA-Seq System (NuGEN Technologies, San Carlos, CA). Briefly, 100 ng of RNA was used to generate cDNA and a strand-specific library following the manufacturer's protocol. In order to deplete contaminating abundant human and *T. gondii* sequences, a cocktail of NuGEN human AnyDeplete rRNA-targeting probes and a custom panel of 196 *T. gondii* AnyDeplete probes were used in order to carry out insert-dependent adaptor cleavage, as described in the manufacturer's protocol. The final cDNA libraries were evaluated on the BioAnalyzer and quantified using the Kapa Library Quantification Kit (Roche Sequencing, Pleasanton, CA) by Molecular Genomics Core Facility (Moffitt Cancer Center, FL). The libraries were then sequenced on the Illumina NextSeq 500 sequencer with 75-base paired-end runs in order to generate at least 10 million read-pairs per sample. Reads were filtered by Sanger quality score using FASTQ Groomer v. 1.0.4 and paired end reads were aligned against the genomes of *T. gondii* (TGME49 version 46; ToxoDB.org) references uploaded into Galaxy using HISAT2. The DESeq2 module was used for normalization, differential gene expression and statistical analysis of uniquely mapped paired-end reads using the default parameters. ME49EW cyst RNA-seq data was compared to ME49 tachyzoite RNA-seq data (r=0.60) kindly provided by ToxoDB. ME49 in vitro bradyzoite (pH8.2-media induction) RNA-seq data, also from ToxoDB, was

compared to the ME49 tachyzoite RNA-seq data (r=0.87). The gene IDs and product descriptions of mRNAs that increased or decreased ≥2 fold in these two comparisons are listed in Dataset S1 along with fold changes of selected growth gene mRNAs.

m*RNA qPCR.* Recrudescing populations were used to infect HFF cells (in duplicate) with 1.5-2 million parasites (MOI 1:1), parasites grown for 24 to 48 hours, and then monolayers were washed in ice cold 1xPBS, scraped on ice in 1xPBS and pelleted at 3800rpm for 15 min at 4°C. The pellet was resuspended in 350μl of RTL buffer and total RNA was purified by manufacturer protocols (RNAeasy kit, Qiagen) RNA was converted to cDNA and purified from each sample by standard methods. The qPCR reaction was: 10μl Luna Universal qPCR master mix (New England bio labs), 0.5μl Primer (of a 10μM stock), 20ng of tachyzoite cDNA or 10ng of cyst cDNA in a 20μl total volume. The amplification program used was 3 min at 95°C, 40 cycles of 10s at 95°C for denaturation and 30s at 60°C for annealing followed by 5s at 65°C and 5s at 95°C for extension finally held at 4°C. See Dataset S1 for all primer designs.

Calculations: Sample $2^{-\Delta Ct}=2^{-(\text{Ct target gene-Ct of ADF control})}$

Relative fold change=$2^{-\Delta Ct}$ sample target gene/$2^{-\Delta Ct}$ Pru-7 value for the same target gene

Cell cycle analyses.

DNA Content. Excysted bradyzoites and freshly lysed and purified RH parasites were pelleted at 2000 rpm for 15 min at 4°C and resuspended in 300μl of cold 70% ethanol in PBS added dropwise. Samples were held at -20°C at least 24 h prior to staining. Samples were pelleted by centrifuging at 6500 rpm for 5 min, the pellet was then resuspended in staining solution [50μM Tris pH 7.5, 1μM SYTOX green (Molecular Probes #S7020) and 1% RNase cocktail] and incubated 30 min at room temperature in the dark. Flow cytometry analysis was performed using a BD-Canto flow cytometer. The cytometer was run in linear mode, calibrated to the 1N population of the RH parasite reference control, and 70,000 events collected per sample. Histograms were generated using FACSDiva software.

Cell cycle IFA. Excysted Bradyzoites were cytospun (500 rpm for 5 min medium acceleration) onto slides, then co-stained for IMC1, centrin and genomic DNA (DAPI) or separately co-stained for

SRS9 and SAG1. IFA analysis of ME49EW Day 2-, 7- and 9-recrudescent populations were also analyzed by IFA using antibodies against IMC1 and centrin and genomic DNA (DAPI). Parasite vacuoles were quantified for single (G1 phase) versus double (S/M phases) centrosomes, and also for the presence of internal daughters in 50 randomly selected vacuoles x3 for each sample.

Hoechst live stain. Purified cysts were stained following brain tissue homogenization using a 1:4 dilution of 12.3mg/ml of Hoechst stain (Thermo Scientific) and incubated for 20-30 minutes prior to being viewed on a Zeiss Axiovert microscope, at 400x magnification and images collected using Zeiss Zen software.

ACKNOWLEDGEMENTS

Toxoplasma gondii genomic and RNA-sequencing data were accessed via http://ToxoDB.org. The authors thank Drs. William Sullivan Jr. and Krista Brooks for their insights and contributions that helped this paper come together. We thank Drs. John Boothroyd, Louis Weiss, and Gary Ward for antibodies used in this study. Tissue cyst RNA-sequencing gene data was generated by the Moffitt Cancer Center Molecular Genomics core facility. This study was supported by NIH NIAID R01 grants AI124682 to MWW and EHW, AI122760 to MWW and DA048815 to EHW.

REFERENCES

1. Dubey JP. 1997. Tissue cyst tropism in Toxoplasma gondii: a comparison of tissue cyst formation in organs of cats, and rodents fed oocysts. Parasitology 115 (Pt 1):15-20.
2. Dubey JP, Frenkel JK. 1976. Feline toxoplasmosis from acutely infected mice and the development of Toxoplasma cysts. J Protozool 23:537-46.
3. Weiss LM, Dubey JP. 2009. Toxoplasmosis: A history of clinical observations. Int J Parasitol 39:895-901.
4. Remington JS. 1974. Toxoplasmosis in the adult. Bull N Y Acad Med 50:211-27.
5. Song HB, Jung BK, Kim JH, Lee YH, Choi MH, Kim JH. 2018. Investigation of tissue cysts in the retina in a mouse model of ocular toxoplasmosis: distribution and interaction with glial cells. Parasitol Res 117:2597-2605.
6. Dellacasa-Lindberg I, Hitziger N, Barragan A. 2007. Localized recrudescence of Toxoplasma infections in the central nervous system of immunocompromised mice assessed by in vivo bioluminescence imaging. Microbes Infect 9:1291-8.

7. Boillat M, Hammoudi PM, Dogga SK, Pages S, Goubran M, Rodriguez I, Soldati-Favre D. 2020. Neuroinflammation-Associated Aspecific Manipulation of Mouse Predator Fear by Toxoplasma gondii. Cell Rep 30:320-334 e6.

8. Odaert H, Soete M, Fortier B, Camus D, Dubremetz JF. 1996. Stage conversion of Toxoplasma gondii in mouse brain during infection and immunodepression. Parasitol Res 82:28-31.

9. Reiter-Owona I, Seitz H, Gross U, Sahm M, Rockstroh JK, Seitz HM. 2000. Is stage conversion the initiating event for reactivation of Toxoplasma gondii in brain tissue of AIDS patients? J Parasitol 86:531-6.

10. Saraf P, Shwab EK, Dubey JP, Su C. 2017. On the determination of Toxoplasma gondii virulence in mice. Exp Parasitol 174:25-30.

11. Brown KM, Sibley LD. 2018. Essential cGMP Signaling in Toxoplasma Is Initiated by a Hybrid P-Type ATPase-Guanylate Cyclase. Cell Host Microbe 24:804-816 e6.

12. Fox BA, Falla A, Rommereim LM, Tomita T, Gigley JP, Mercier C, Cesbron-Delauw MF, Weiss LM, Bzik DJ. 2011. Type II Toxoplasma gondii KU80 knockout strains enable functional analysis of genes required for cyst development and latent infection. Eukaryot Cell 10:1193-206.

13. Watson GF, Davis PH. 2019. Systematic review and meta-analysis of variation in Toxoplasma gondii cyst burden in the murine model. Exp Parasitol 196:55-62.

14. Watts E, Zhao Y, Dhara A, Eller B, Patwardhan A, Sinai AP. 2015. Novel Approaches Reveal that Toxoplasma gondii Bradyzoites within Tissue Cysts Are Dynamic and Replicating Entities In Vivo. mBio 6:e01155-15.

15. Sahm M, Fischer HG, Gross U, Reiter-Owona I, Seitz HM. 1997. Cyst formation by Toxoplasma gondii in vivo and in brain-cell culture: a comparative morphology and immunocytochemistry study. Parasitol Res 83:659-65.

16. Radke JR, Striepen B, Guerini MN, Jerome ME, Roos DS, White MW. 2001. Defining the cell cycle for the tachyzoite stage of Toxoplasma gondii. Mol Biochem Parasitol 115:165-75.

17. Radke JR, Guerini MN, Jerome M, White MW. 2003. A change in the premitotic period of the cell cycle is associated with bradyzoite differentiation in Toxoplasma gondii. Mol Biochem Parasitol 131:119-27.

18. Schluter D, Barragan A. 2019. Advances and Challenges in Understanding Cerebral Toxoplasmosis. Front Immunol 10:242.

19. Ndubuizu O, LaManna JC. 2007. Brain tissue oxygen concentration measurements. Antioxid Redox Signal 9:1207-19.

20. Jerome ME, Radke JR, Bohne W, Roos DS, White MW. 1998. Toxoplasma gondii bradyzoites form spontaneously during sporozoite-initiated development. Infect Immun 66:4838-44.

21. Su C, Howe DK, Dubey JP, Ajioka JW, Sibley LD. 2002. Identification of quantitative trait loci controlling acute virulence in Toxoplasma gondii. Proc Natl Acad Sci U S A 99:10753-8.

22. Joyce BR, Queener SF, Wek RC, Sullivan WJ, Jr. 2010. Phosphorylation of eukaryotic initiation factor-2{alpha} promotes the extracellular survival of obligate intracellular parasite Toxoplasma gondii. Proc Natl Acad Sci U S A 107:17200-5.

23. Garfoot AL, Wilson GM, Coon JJ, Knoll LJ. 2019. Proteomic and transcriptomic analyses of early and late-chronic Toxoplasma gondii infection shows novel and stage specific transcripts. BMC Genomics 20:859.

24. Mordue DG, Monroy F, La Regina M, Dinarello CA, Sibley LD. 2001. Acute toxoplasmosis leads to lethal overproduction of Th1 cytokines. J Immunol 167:4574-84.

25. Lindsay DS, Dubey JP, Blagburn BL, Toivio-Kinnucan M. 1991. Examination of tissue cyst formation by Toxoplasma gondii in cell cultures using bradyzoites, tachyzoites, and sporozoites. J Parasitol 77:126-32.

26. Shukla A, Olszewski KL, Llinas M, Rommereim LM, Fox BA, Bzik DJ, Xia D, Wastling J, Beiting D, Roos DS, Shanmugam D. 2018. Glycolysis is important for optimal asexual growth and formation of mature tissue cysts by Toxoplasma gondii. Int J Parasitol 48:955-968.

27. Kim SK, Boothroyd JC. 2005. Stage-specific expression of surface antigens by Toxoplasma gondii as a mechanism to facilitate parasite persistence. J Immunol 174:8038-48.

28. Radke JB, Worth D, Hong D, Huang S, Sullivan WJ, Jr., Wilson EH, White MW. 2018. Transcriptional repression by ApiAP2 factors is central to chronic toxoplasmosis. PLoS Pathog 14:e1007035.

29. Sugi T, Ma YF, Tomita T, Murakoshi F, Eaton MS, Yakubu R, Han B, Tu V, Kato K, Kawazu S, Gupta N, Suvorova ES, White MW, Kim K, Weiss LM. 2016. Toxoplasma gondii Cyclic AMP-Dependent Protein Kinase Subunit 3 Is Involved in the Switch from Tachyzoite to Bradyzoite Development. mBio 7.

30. Gubbels MJ, Lehmann M, Muthalagi M, Jerome ME, Brooks CF, Szatanek T, Flynn J, Parrot B, Radke J, Striepen B, White MW. 2008. Forward genetic analysis of the apicomplexan cell division cycle in Toxoplasma gondii. PLoS Pathog 4:e36.

31. Jeffers V, Tampaki Z, Kim K, Sullivan WJ, Jr. 2018. A latent ability to persist: differentiation in Toxoplasma gondii. Cell Mol Life Sci 75:2355-2373.

32. Rani S, Cerqueira-Cezar CK, Murata FHA, Sadler M, Kwok OCH, Pradhan AK, Hill DE, Urban JF, Jr., Dubey JP. 2019. Toxoplasma gondii tissue cyst formation and density of tissue cysts in shoulders of pigs 7 and 14 days after feeding infected mice tissues. Vet Parasitol 269:13-15.

33. Dubey JP. 2005. Unexpected oocyst shedding by cats fed Toxoplasma gondii tachyzoites: in vivo stage conversion and strain variation. Vet Parasitol 133:289-98.

34. Luder CGK, Rahman T. 2017. Impact of the host on Toxoplasma stage differentiation. Microb Cell 4:203-211.

35. Ferguson DJ, Hutchison WM. 1987. An ultrastructural study of the early development and tissue cyst formation of Toxoplasma gondii in the brains of mice. Parasitol Res 73:483-91.

36. Cabral CM, Tuladhar S, Dietrich HK, Nguyen E, MacDonald WR, Trivedi T, Devineni A, Koshy AA. 2016. Neurons are the Primary Target Cell for the Brain-Tropic Intracellular Parasite Toxoplasma gondii. PLoS Pathog 12:e1005447.

37. Radke JR, Donald RG, Eibs A, Jerome ME, Behnke MS, Liberator P, White MW. 2006. Changes in the expression of human cell division autoantigen-1 influence Toxoplasma gondii growth and development. PLoS Pathog 2:e105.

38. Xue Y, Theisen TC, Rastogi S, Ferrel A, Quake SR, Boothroyd JC. 2020. A single-parasite transcriptional atlas of Toxoplasma gondii reveals novel control of antigen expression. Elife 9.

39. Roos DS, Donald RG, Morrissette NS, Moulton AL. 1994. Molecular tools for genetic dissection of the protozoan parasite Toxoplasma gondii. Methods Cell Biol 45:27-63.

40. Dubey JP. 1980. Mouse pathogenicity of Toxoplasma gondii isolated from a goat. Am J Vet Res 41:427-9.

41. Buchholz KR, Fritz HM, Chen X, Durbin-Johnson B, Rocke DM, Ferguson DJ, Conrad PA, Boothroyd JC. 2011. Identification of tissue cyst wall components by transcriptome analysis of in vivo and in vitro Toxoplasma gondii bradyzoites. Eukaryot Cell 10:1637-47.

FIGURES IN ORDER OF APPEARANCE

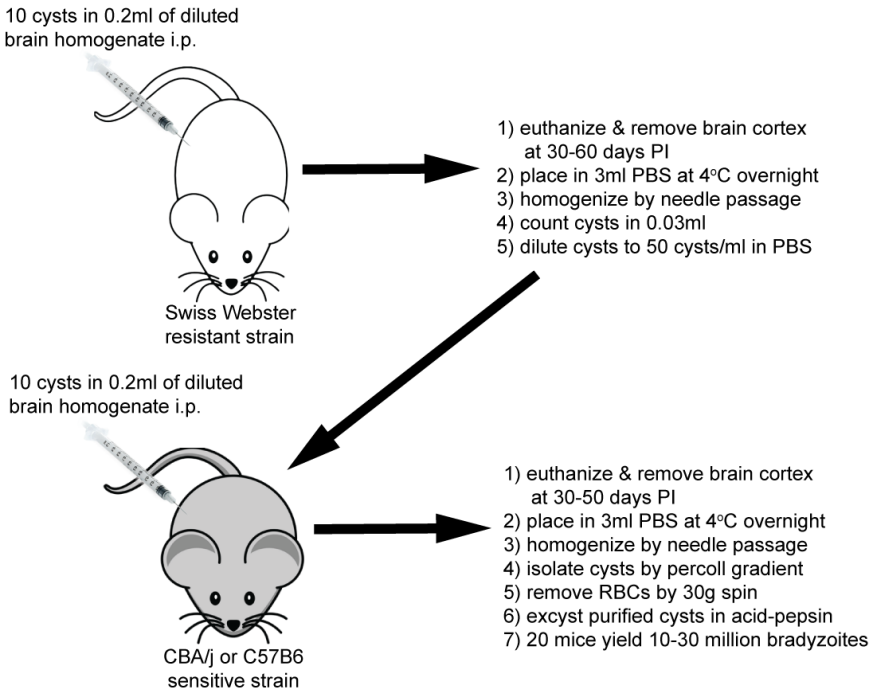

Figure S1. ME49EW tissue cyst maintenance and production.
The ME49EW strain is maintained in the relatively resistant Swiss Webster (SWR/j) mouse strain by a 10 cyst inoculation (i.p.) every 30-60 days. Tissue cysts from Swiss Webster brain homogenates are used to amplify tissue cysts numbers in the sensitive CBA/j mouse strain (30-50 day infections). Sequential passage in CBA/j mice alone results in a progressive decline in tissue cyst number after multiple passages. The major steps for maintenance and experimental procedures are indicated with full details in Materials and Methods.

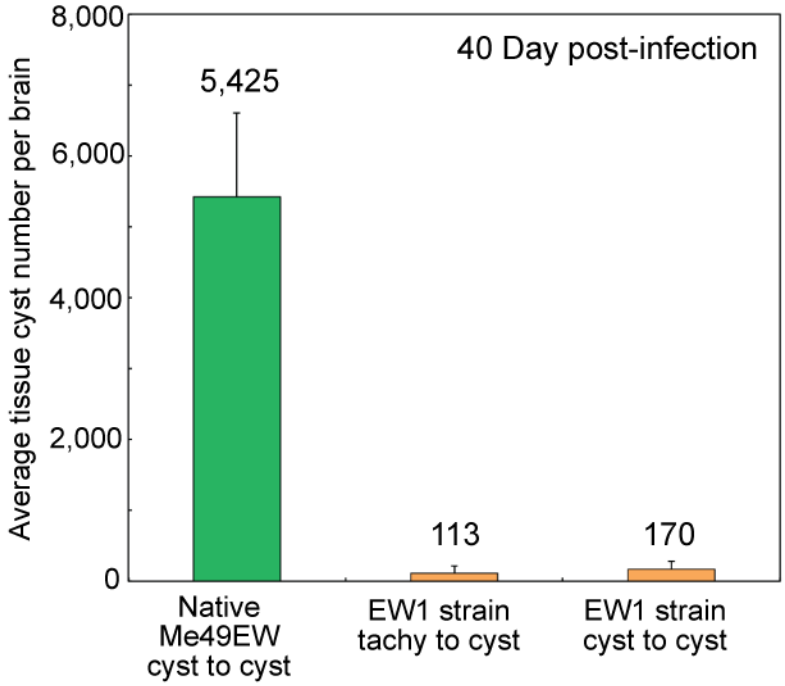

Figure 1. Adaptation to growth in HFF cell culture leads to a permanent loss of in vivo developmental competency.
The Type II strain, ME49EW, maintained in mice (see Fig. S1) and an HFF-adapted strain derived from this strain, ME49EW1, were used to infect 15 CBA/j mice. Infections: 10 tissue cysts of the native ME49EW strain in PBS-diluted brain homogenate (see Materials and Methods) were inoculated (i.p.) into each mouse of a group of 5 (native ME49EW cyst to cyst); ME49EW1 tachyzoites were inoculated (10k tachyzoites/mouse i.p.) into 5 mice (EW1 tachy to cyst); and finally, ME49EW1 tissue cysts (10 cysts, i.p.) from the tachy-to-cyst infected mice were used to infect 5 mice (EW1 cyst to cyst). Brain tissue homogenates (3 ml) were prepared 40 day post-infection and total tissue cysts in 0.030 ml aliquots (1/100th of homogenate) were enumerated in at least triplicate by direct microscopic examination. Numbers above each bar=average cyst number.

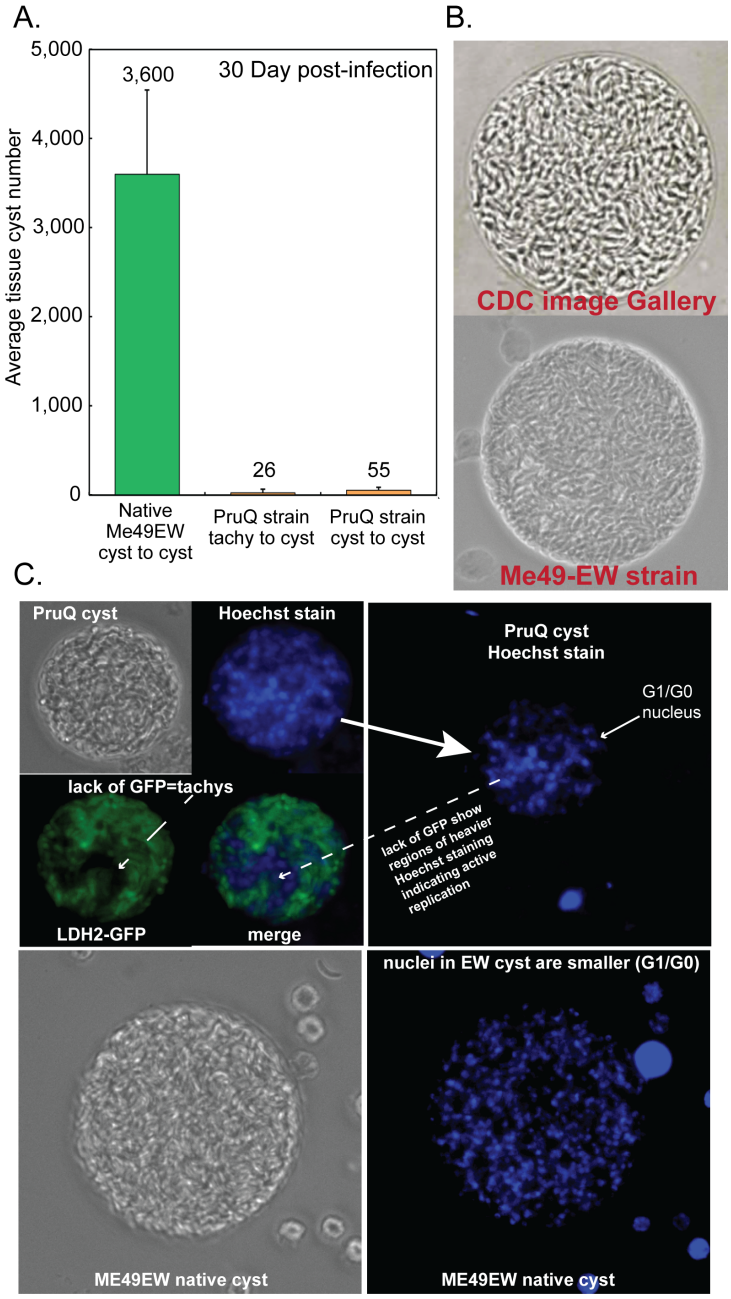

Figure S2. Comparison of ME49EW and PruQ tissue cysts.
[A.] ME49EW and PruQ parasites were used to infect CBA/j mice and tissue cysts in brain homogenates determined at 30 day post-infection. (PruQ=Prugnauid*Δku80Δhxgprt* ::LDH2-GFP) Infections: 10 tissue cysts of the native ME49EW strain in PBS-diluted brain homogenate were inoculated (i.p.) into each mouse of a group of 4 (native ME49EW cyst to cyst). PruQ strain tachyzoites were inoculated (10k parasites/mouse i.p.) into 4 mice (PruQ tachy to cyst). PruQ tissue cysts (10 cysts, i.p.) from the tachy-to-cyst infected mice above were used to infect 3 mice (PruQ cyst to cyst). Brain tissue homogenates (3 ml) were prepared and total tissue cysts in 0.030 ml aliquots (1/100th of homogenate) enumerated in a least triplicate by direct microscopic examination. Number above each bar=average number of cysts. Note: A consistent 1.5 fold increase in tissue cyst number is observed between 30-40 days in ME49EW CBA/j mouse-infections; compare the average cyst number here to the 40 day PI of Fig. 1. **[B.]** A representative example of a live ME49EW cyst (400x, DIC image) compared to CDC cyst image (https://www.cdc.gov/dpdx/toxoplasmosis/index.html). **[C.]** Representative DIC and fluorescence images of live tissue cysts stained with Hoechst dye (top image row=PruQ and bottom row=ME49EW. All images are 400x magnification and were captured using the same mode fluorescent settings. Green=live bradyzoites (tachyzoites do not fluoresce), Blue=live Hoechst staining of genomic DNA. Note that PruQ cysts are substantially smaller than ME49EW cysts at 30 day PI and contain large gaps in GFP fluorescence. The right hand Hoechst stained images for PruQ and ME49EW were adjusted identically to reduce fluorescent signal spreading in order to better capture nuclei size and relative DNA content. Note the small nuclei consistent with G1/G0 parasites (see Fig. S3) are uniform and numerous in the ME49EW cyst. The nuclei in the PruQ cyst are nonuniform with large nuclei staining more intensely and co-localized with the gaps in the LDH2-GFP fluorescence suggesting these are replicating tachyzoites. Smaller nuclei are associated with the regions of GFP fluorescence in the PruQ cyst consistent with bradyzoites.

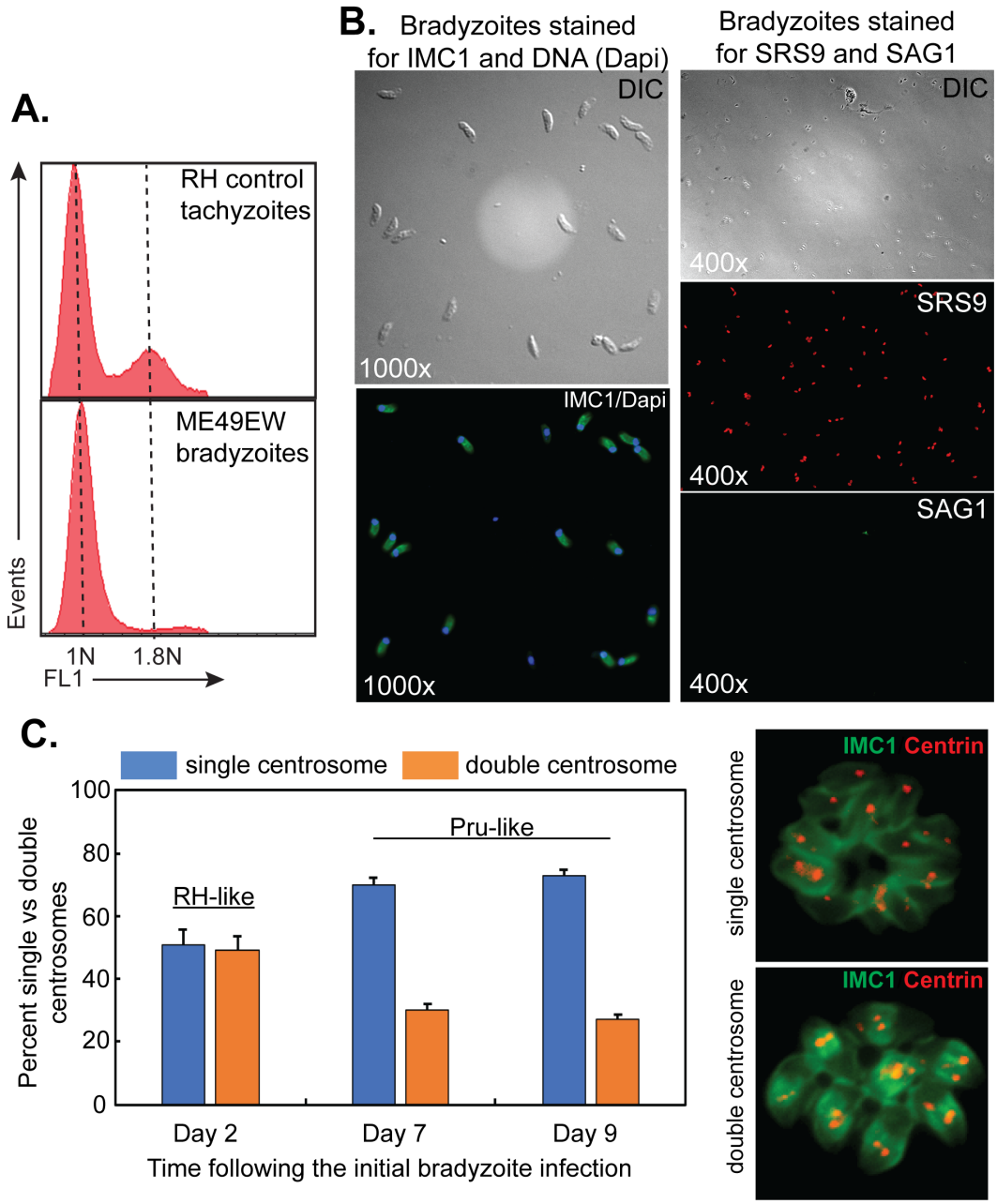

Figure S3. Cell cycle analysis of ME49EW parasite populations.
[A.] Genomic DNA analysis of ME49EW bradyzoites in comparison to RH tachyzoites. Parasites were purified, ethanol fixed and stained with SYTOX dye and analyzed by FACS. The cytometer was set to linear mode fluorescence and calibrated to the asynchronous RH control parasites; dashed lines reference 1N and 1.8N fluorescence peaks in the asynchronous control. DNA fluorescence was measured in FL-1 (x-axis) and 70,000 events (y-axis) were collected for each histogram. **[B.]**. Representative images of ME49EW bradyzoites co-stained for IMC1 and Dapi or separately co-stained for SRS9 and SAG1. Note all bradyzoites were SRS9+/SAG1- but lack evidence of mitosis (internal IMC1 daughters or reduplicated nuclear forms). The IMC1-Dapi merge image shown is representative of ~1,000 bradyzoites examined. **[C.]** At Day 2 (first monolayer), 7 (3rd monolayer), and 9 (4th monolayer) from the initial bradyzoite infection, parasites were fixed and co-stained for anti-centrin (centrosome), Dapi (DNA), and anti-IMC1 (internal daughters). Single versus double centrosomes were quantified in 50x3 vacuoles selected at random. The merged images (IMC1 and Centrin co-staining) to the right are representative of parasites possessing single versus double centrosomes.

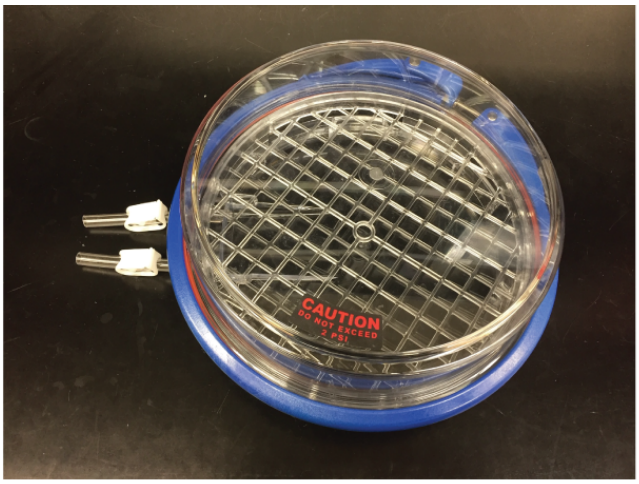

Native bradyzoites in mouse brain reside in a hypoxic tissue environment, and as a consequence ME49EW strain bradyzoite-infected HFF monolayers are healthier if cultured at 37°C under 5% oxygen in HEPES buffered DMEM media containing 5% FBS (media recipe below). To achieve hypoxia conditions we use a hypoxia chamber (see picture) charged with mixed gas 90% nitrogen/5% oxygen/5% CO2 for 3 min and placed on the shelf of a CO2 incubator at 37°C. Using a multi-gas incubator commonly used to propagate *Plasmodium falciparum* merozoites in RBCs would also work.
[Hypoxia chambers, https://www.stemcell.com/hypoxia-incubator-chamber.html]

Growth media recipe for HFF and neonatal cells:
Volume: 500ml
--Use power DMEM media with L-glutamine and sodium pyruvate (6.74g),
--add 12.5ml 1M HEPES buffer, 25ml FBS, and 5 ml of antibiotic mix (Pen-strep and amphotericin B).
--For astrocyte media, add 1% GlutaMAX supplement
--Make the full media, then bring up to 37°C and adjust pH to 7.4 using 4M KOH.
--Sterile filter.

Figure S4. Cell culture of native *Toxoplasma* ME49EW parasites.

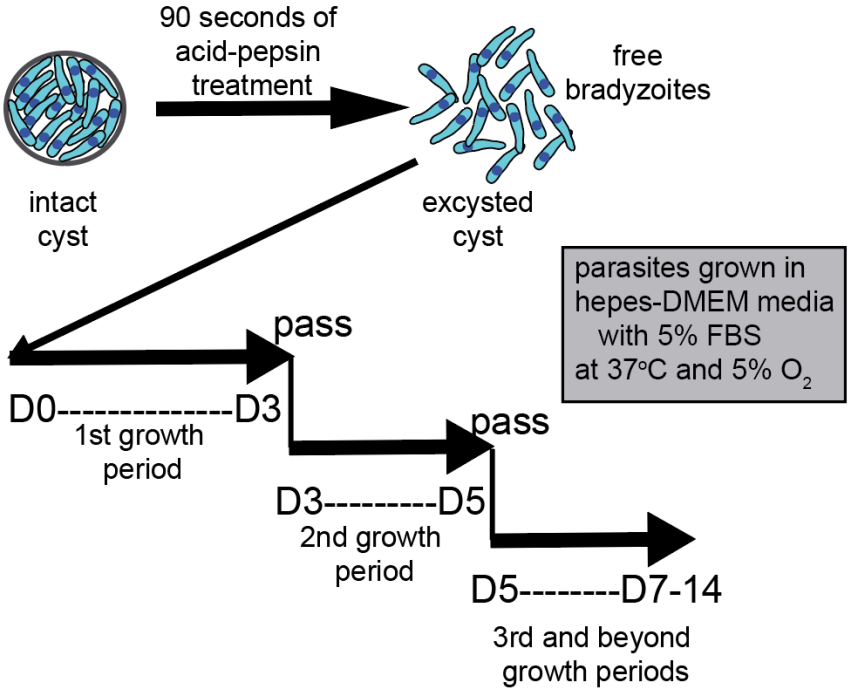

Figure S5. Experimental methods for establishing an ex vivo recrudescence model.
Parasite populations are followed for 1-2 weeks and are labeled by the cumulative time from the original bradyzoite infection (D0). For example, Day 3-populations are the end point of the cultures infected with bradyzoites; Day 5-populations are the end point of the cultures infected with Day 3 parasites; Day 7-populations are the end point of cultures of infected with Day 5 parasites etc. In previous studies of sporozoite-initiated development of the Type III, VEG strain the number of passages had no effect on the course of parasite development in HFF cells (20).

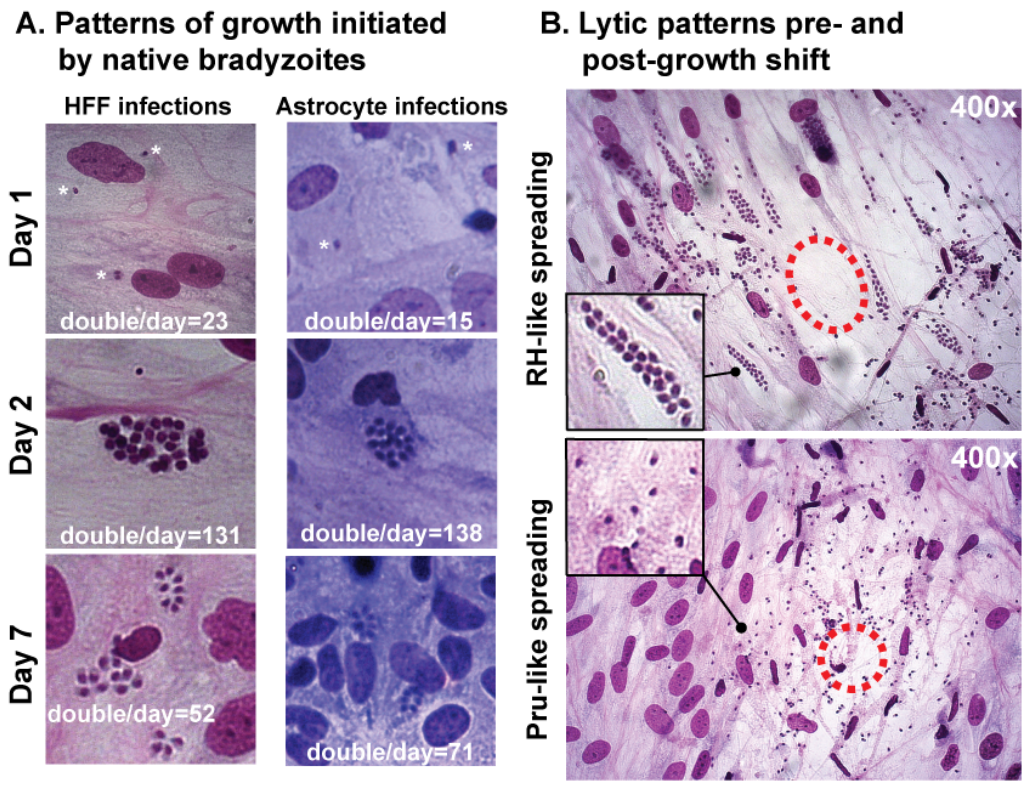

C. Population growth changes

Human foreskin fibroblasts					
Day Innoculated	**# of Parasites Inoculated**	**Day Harvested**	**# of Parasites Harvested**	**TL Fold Change**	**Fold per Day**
Day 0	3 million	**Day 3**	23 million	7.67	2.55
Day 3	9 million	**Day 5**	64 million	7.11	3.55
Day 5	50 million	**Day 8**	52 million	1.04	0.34
Day 8	50 million	**Day 12**	40 million	0.80	0.20
Mouse astrocytes					
Day 0	5 million	**Day 3**	33 million	6.51	2.17
Day 3	8 million	**Day 5**	53 million	6.60	3.3
Day 5	48 million	**Day 7**	23 million	0.48	0.24
Day 7	8 million	**Day 9**	22 million	2.80	1.4
Day 9	8 million	**Day 14**	35 million	4.43	0.886

Figure 2. Native ME49EW bradyzoites initiate a dynamic developmental process. ME49EW bradyzoites from CBA/j murine brain tissue cysts were purified and used to inoculate monolayers of HFF cells or neonatal murine astrocytes (see Materials and Methods). At various times, H&E stains (nuclei stain dark blue to violet) were prepared and vacuole size and lytic patterns were evaluated. **[A.]** Representative images of the major vacuole sizes. Total doublings (e.g. vacuole of 32=5 doublings) in 50 randomly selected vacuoles were determined in triplicate and the average parasite doublings per day are indicated at the bottom of each image. Note: Day 1-populations showed minimal growth (astrocytes=70% singles; HFF=60% singles), therefore, we subtracted Day 1 doublings from Day 2-population values in order to estimate the average doublings from the end of Day 1 to the end of Day 2. Asterisks in the top two images indicate the single bradyzoite vacuoles. **[B.]** Representative lytic patterns of Day 3- and Day 11-populations in HFF cells (first and fourth growth periods, see Fig. S5). Dashed circles indicate the approximate center of each plaque. Inset images=higher magnification of equal areas of the plaque, note the nuclei size differences and relative MOI in each plaque. **[C.]** Representative net population growth during each growth period in HFF or astrocyte monolayers are shown. The growth periods ranged from 2 to 5 days as indicated and Day 0 corresponds to the starting bradyzoite infection.

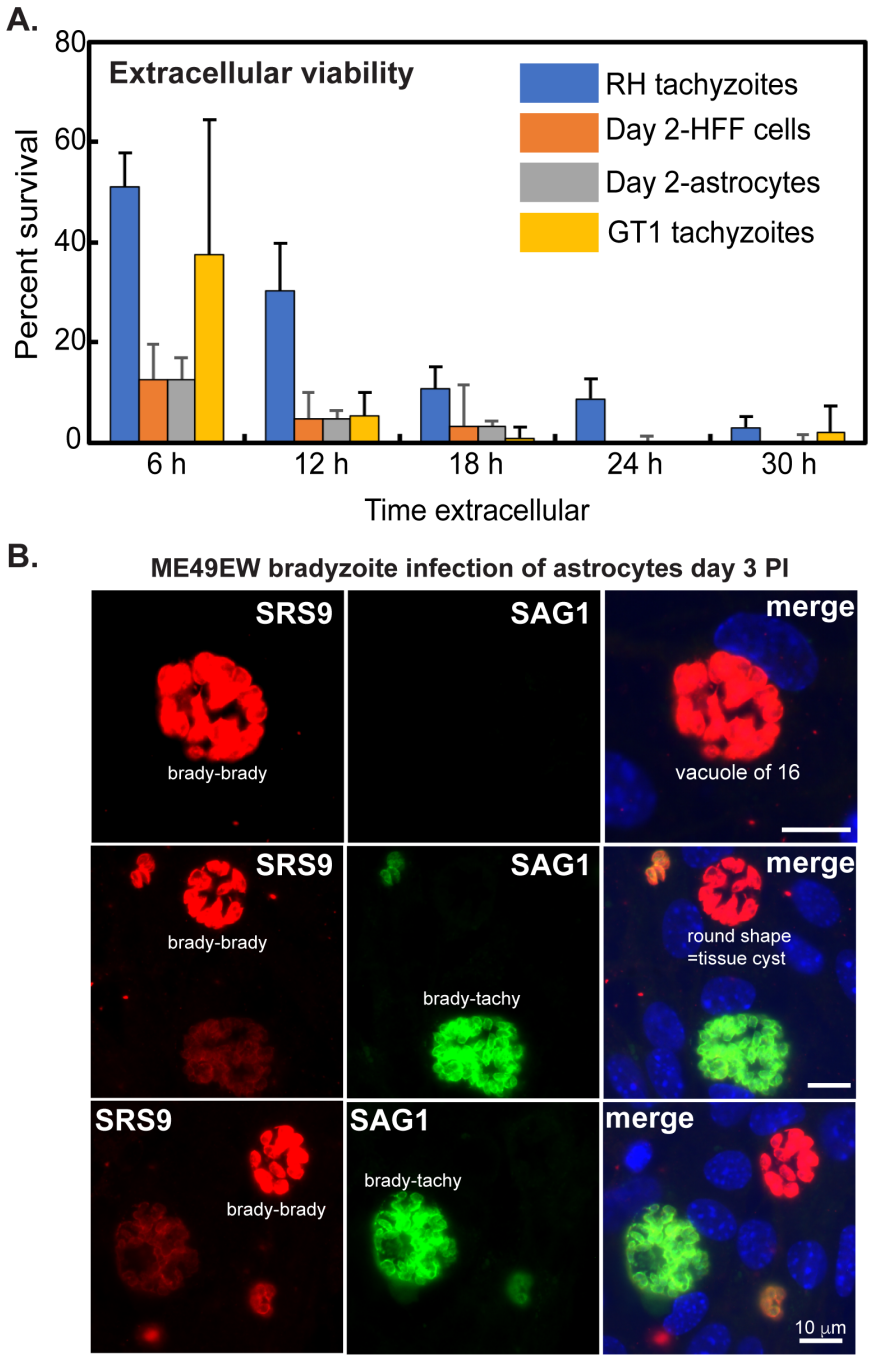

Figure S6. Extracellular half-life and examples of bradyzoite-to bradyzoite replication. **[A.]** Day 2-recrudescence populations from ME49EW bradyzoite infections of HFF or astrocyte monolayers and Type I, RH and GT1 strain tachyzoites were purified by standard methods and free parasites were resuspended at 1 million/ml of media and incubated at 37°C. At time zero, and every 6 h through 30 h, 10,000 parasites were sampled and used to infect duplicate cover slips. After 48 h of further growth (beyond the last 30 h time point), the cover slips were fixed and stained with goat, anti-*Toxoplasma* antibody and the number of plaques in 10 microscopic fields determined in triplicate (6 total counts/timepoint). All results were plotted as a percent of the number of plaques as compared to the time-zero plaque values. **[B.]** Additional examples of bradyzoite to bradyzoite replication (SRS9+/SAG1-) occurring along side bradyzoite to tachyzoite replication in neonatal astrocytes infected with ME49EW bradyzoites. merge image=co-staining for SRS9 and SAG1 and Dapi, which stains the large astrocyte nucleus. Note the smooth boundary and round shape of the SRS9+ vacuole in the middle panel consistent with a tissue cyst wall. See Figure 3C for an additional example and method details.

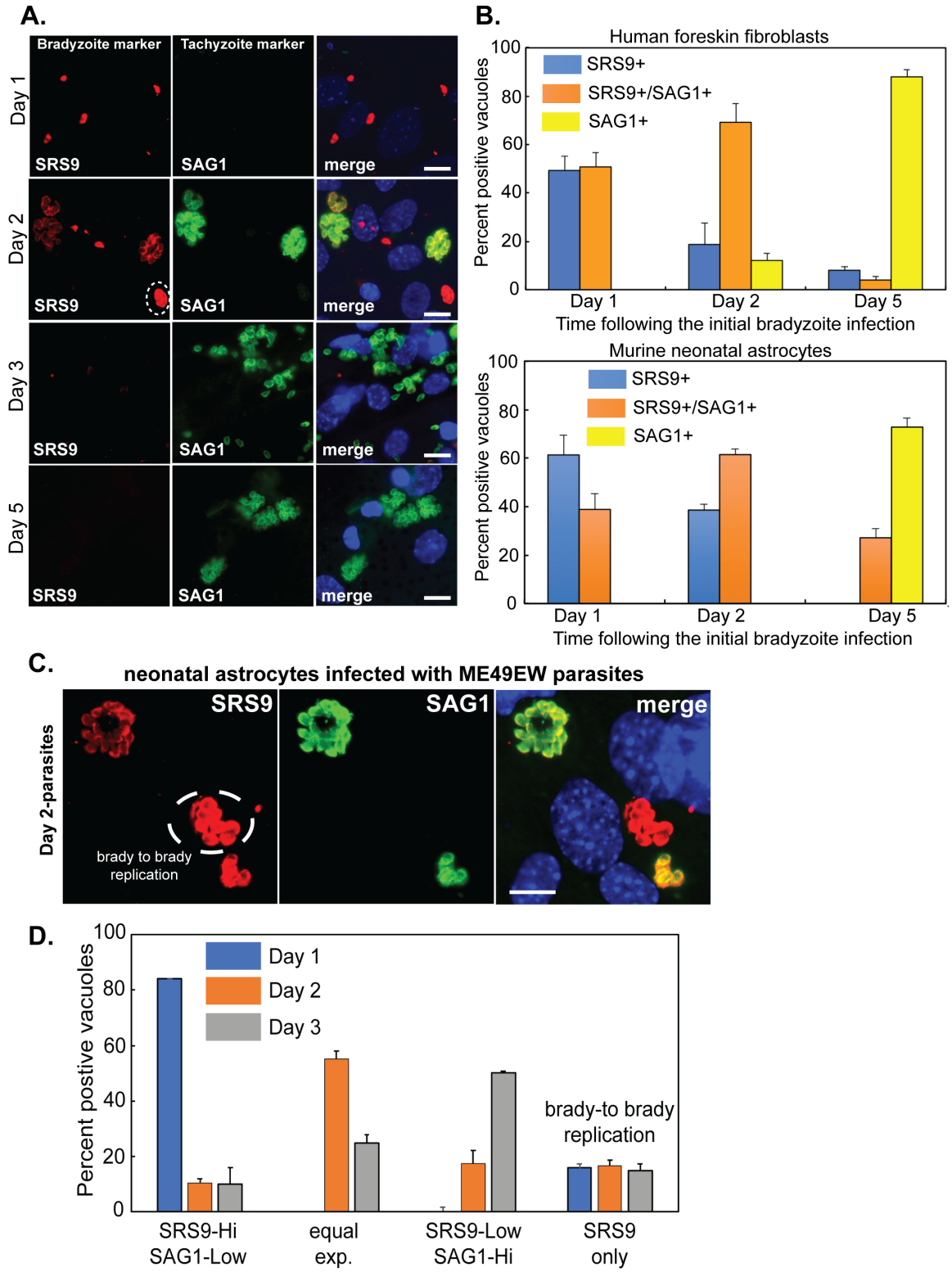

Figure 3. Changes in bradyzoite and tachyzoite surface antigen expression.
SAG1 and SRS9 are developmentally regulated SRS antigens specific for tachyzoite and bradyzoite stages, respectfully. At various times following an initial bradyzoite infection of HFF (see Supplemental Fig. S7 for representative images) or astrocyte monolayers, IFA analysis was performed using co-stains for SAG1 (green), SRS9 (red) and Dapi (DNA, blue). **[A.]** Representative images of parasite staining patterns Day 1-3 post-infection of neonatal astrocytes with native bradyzoites. Day 5-images were of astrocyte monolayers infected with parasites purified from the Day 3-astrocyte culture and grown for 48

h. Note the dashed circle in the Day 2-image is a SRS9-Hi/SAG1-low vacuole, while the other three replicating vacuoles in this microscope field are SRS9-low/SAG1-Hi. Note also the SRS9 only single parasite vacuole in this field. Scale bars=10 μm **[B.]** Parasite vacuoles in HFF cells or astrocytes expressing SAG1 and/or SRS9 were quantified at the indicated times. The SRS9-only vacuoles (blue bar) in HFF cells were single parasite vacuoles, there was no evidence of bradyzoite to bradyzoite replication observed in HFF cell IFAs. Note: quantification of SAG1 and/or SRS9 expression in Day 3 vacuoles is not included due to the extensive host cell lysis. **[C.]** Representative images of bradyzoite to bradyzoite replication (dashed circle) from a Day 2-astrocyte cell culture (vacuole of 8 parasites). For additional examples, see Figure S6B. Bradyzoite replication was not observed in HFF infected cell cultures. Parasites were co-stained for SRS9 (red), SAG1 (green) and Dapi (merged image shows host cell nuclei). Scale bars=10 μm **[D.]** Quantification of the developmental patterns of replicating vacuoles (≥ 2 parasites/vacuole) in bradyzoite-infected astrocytes over three days.

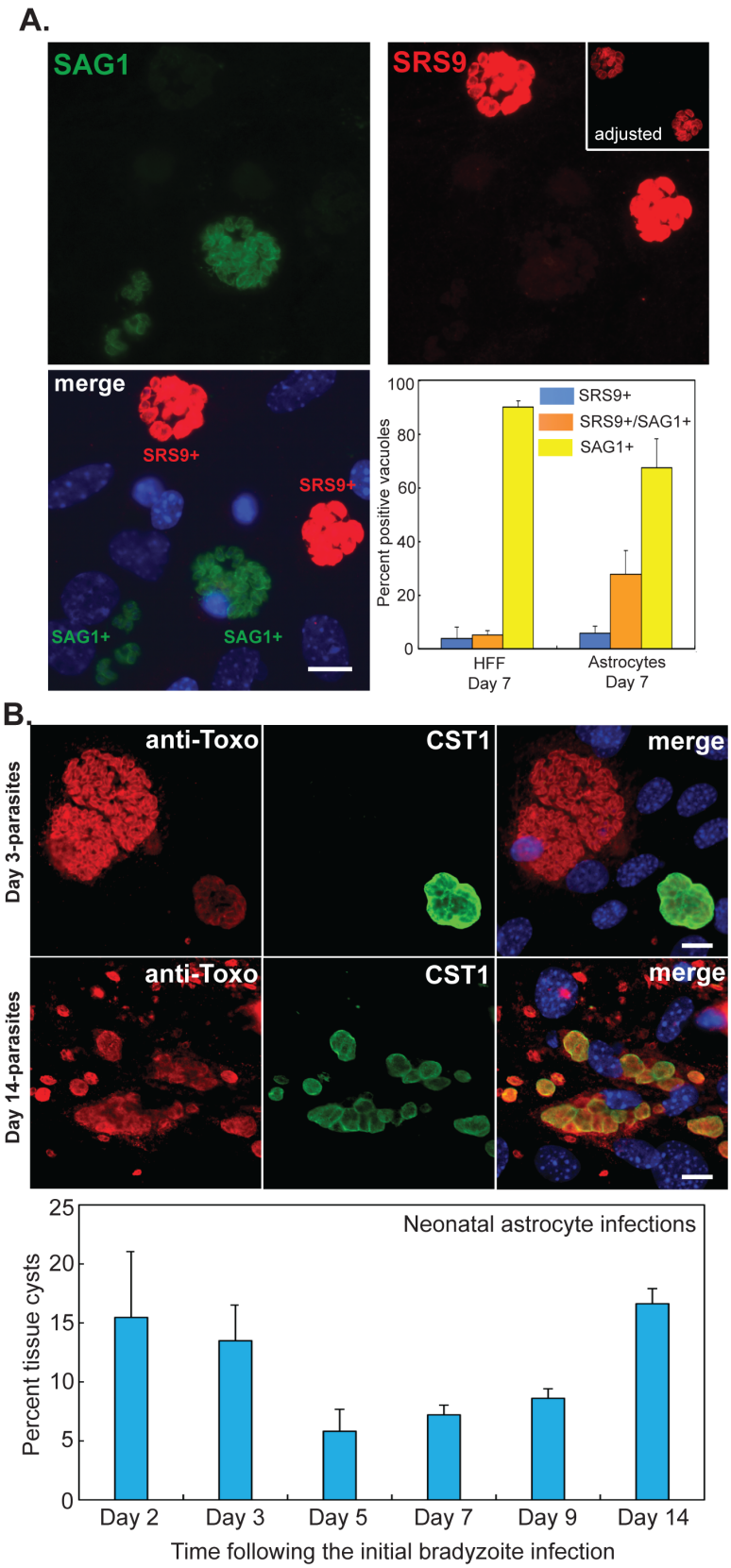

Figure 4. Post-growth shift development and assembly of cyst walls in astrocytes. [A.] SRS9 expression was assessed by IFA in post-growth shift infected astrocytes (Day 7-populations. 3rd growth period, Fig. S5). Infected astrocytes were fixed and co-stained for SAG1 (green) and SRS9 (red) with Dapi staining included as a reference (DNA, blue). Representative images of SAG1+ or SRS9+ only parasite vacuoles in astrocyte-infected cells. Scale bars=10 μm Note two levels of SRS9 fluorescence are shown; the main images display the relative SRS9 to SAG1 fluorescence signal, while the inset box displays a lower mode fluorescence for SRS9 that more clearly shows individual parasites in these vacuoles. Graph: quantification of SRS9 only, SRS9 & SAG1, or SAG1 only in Day 7-populations in HFF or astrocyte cells is also shown. Note that the Day 7-populations (3rd monolayers) in HFF cells have higher levels of SAG1 only vacuoles. There are also rare SRS9 only vacuoles (blue bar) containing single parasites (~1/5 of the 20% single parasite vacuoles in the HFF cultures). By contrast, there were no single parasite vacuoles observed in the astrocyte Day 7-cultures. **[B.]** Representative images of tissue cysts in ME49EW infected astrocytes at Day 3 (first growth period) and Day 14 (fourth growth period) from the original ME49EW bradyzoite infection. CST1 staining (green), anti-*Toxoplasma* (red), and Dapi (blue). Scale bars= 10 μm. Note the Day 3-image shows a single cysts along side two large vacuoles of rapidly growing tachyzoites that dominates these cultures. The cluster of cysts in the Day 14 image highlights the focal nature of some cyst formation in these cultures. Graph: quantitation of the average percent of vacuoles containing a tissue cyst wall at various times from the original bradyzoite infection. Growth/monolayer periods: Day 0-3, Day 3-5, Day 5-7, Day 9-14. Note that CST1 expression and spontaneous assembly into a cyst wall occurred in <1% of vacuoles in all HFF infected cultures.

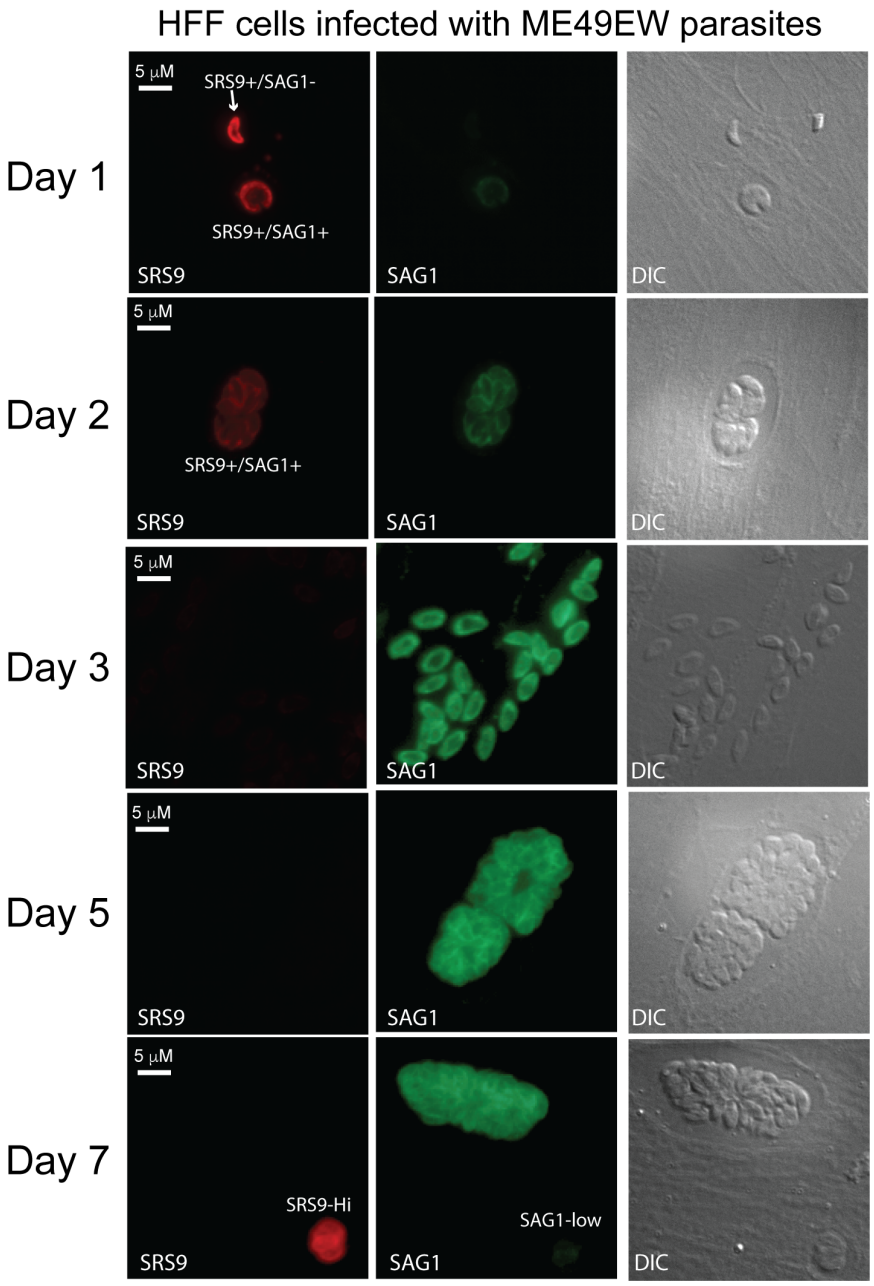

Figure S7. Changes in parasite developmental antigen expression in HFF cells.
Representative images of parasite staining patterns Day 1-3 post-infection of HFF cells infected with native bradyzoites purified from mouse brain. Day 5 and Day 7 images were of HFF cells infected with parasites purified from Day 3- or Day 5-parasite populations and then grown for 48 h to yield Day 5-images and Day 7-images, respectively. Parasites were fixed and co-stained for SAG1 (green), SRS9 (red). Paired DIC images are shown on the right.

A.

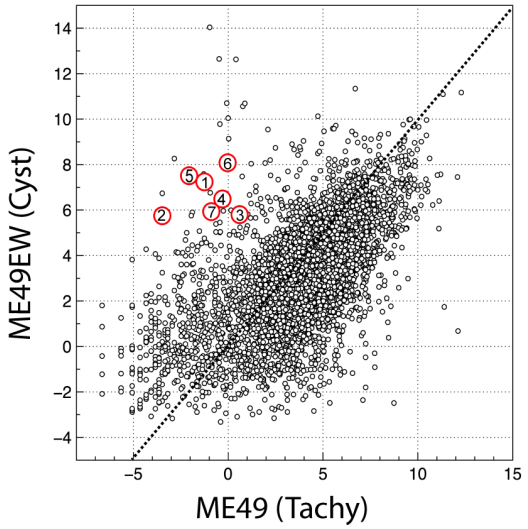

B.

Bradyzoite RNA-seq data reported as fold increase over ME49 tachyzoite mRNA levels (pH7.2 media)

graph #	Gene ID TEME49_	28 Day Cysts	ME49EW 40 day Cysts	ME49 pH8.2
1	202025	2.43	359.29	17.10
2	207130	208.59	597.88	32.33
3	207160	147.71	36.60	4.6
4	220560	409.50	110.66	2.28
5	221840	37.63	759.44	40.92
6	238440	417.89	275.85	14.12
7	258370	1250.09	112.95	1.46

C.

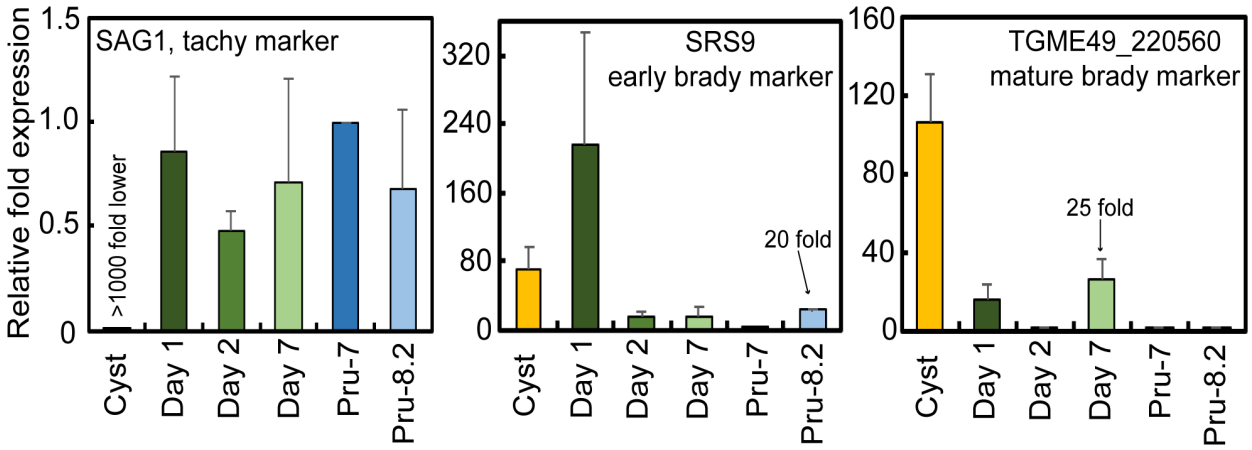

Figure 5. Native bradyzoite gene expression in ME49EW in vivo tissue cysts.
[A.and B.] Graph: analysis of whole-cell mRNA expression of Type II, ME49EW tissue cysts at 40 day post-infection in comparison to ME49 tachyzoites (r=0.60). Table: a small list of highly expressed in vivo-specific ME49EW tissue cyst mRNAs (fold change values) are compared to the fold changes for these same genes in 28 day-in vivo tissue cysts (23) and ME49 alkaline-induced in vitro parasites (pH8.2 media). See Materials and Methods for full details. The order number for the seven in vivo tissue cyst mRNAs are indicated by a numbered red circle in the graph. **[C.]** qPCR gene expression analysis of SAG1, SRS9, and the in vivo-specific tissue cyst gene, TGME49_220560 (unknown protein). Results are presented as relative fold expression over the corresponding PruQ tachyzoite $2^{-\Delta Ct}$ values. RNA sources: ME49EW tissue cysts and Day 1-, 2-, and 7-recrudescent populations grown in HFF cells; PruQ strain tachyzoites (Pru-7) and PruQ tachyzoites induced to differentiate in pH8.2 media (Pru-8.2).

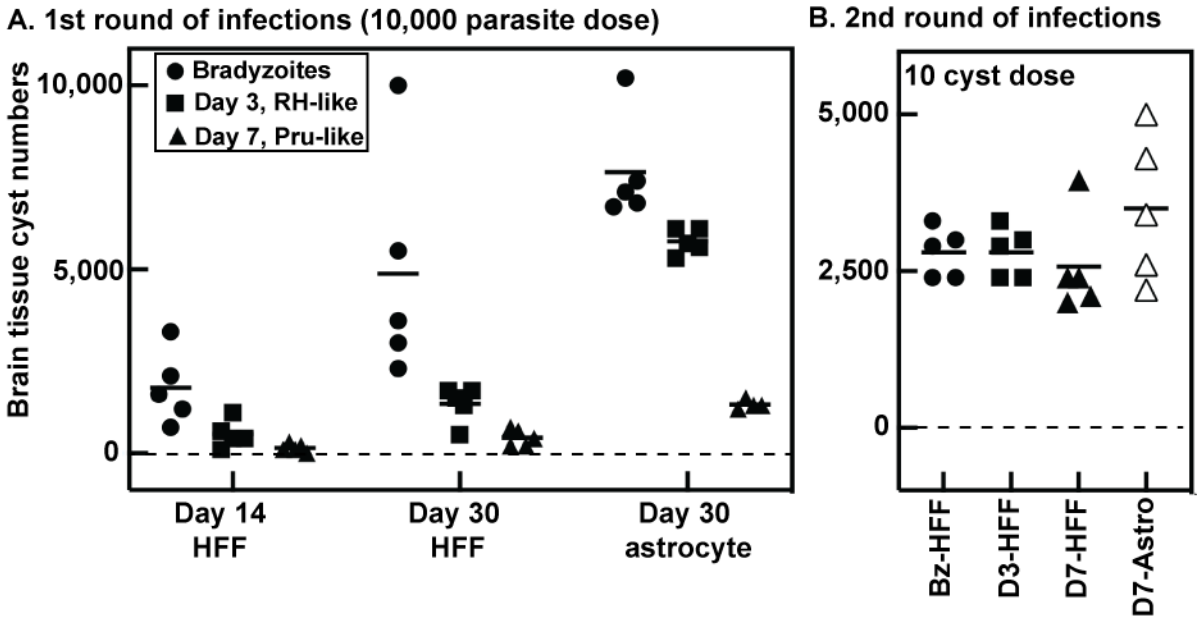

Figure 6. ME49EW parasites post-growth shift produce lower tissue cyst numbers in mouse brain.
Native ME49EW bradyzoites were obtained from tissue cysts purified from mouse brain tissue (closed circles). Bradyzoite infection of HFF or astrocyte cells was used to obtain RH-like, Day 3 tachyzoites (closed squares). Passage of Day 5-parasites into HFF or astrocytes provided Pru-like, Day 7 tachyzoites (closed triangles). **[A.]** Groups of 5 CBA/j mice (45 total) were used to evaluate tissue cyst numbers in brain tissue at Day 14 or Day 30 post-infection. Infections: 10k bradyzoites/mouse inoculated i.p. with counts at Day 14 and Day 30 post-infection (two independent cyst preparations); 10k Day 3-parasites inoculated i.p., with counts at Day 14 (only HFF-derived parasites) and Day 30 post-infection (HFF- or astrocyte-derived); 10k Day 7-parasites i.p., with counts Day 14 (only HFF-derived) and Day 30 post-infection (HFF- or astrocyte-derived). **[B.]** Tissue cysts from Day 30 PI mice infected in [A.] with bradyzoites, Day 3-parasites, or Day 7-parasites (HFF- or astrocyte-derived is indicated) were used to infect new groups of CBA/j mice (5 mice/group, 25 total); 10 cysts inoculated i.p., with tissue cyst counts at Day 30 PI.

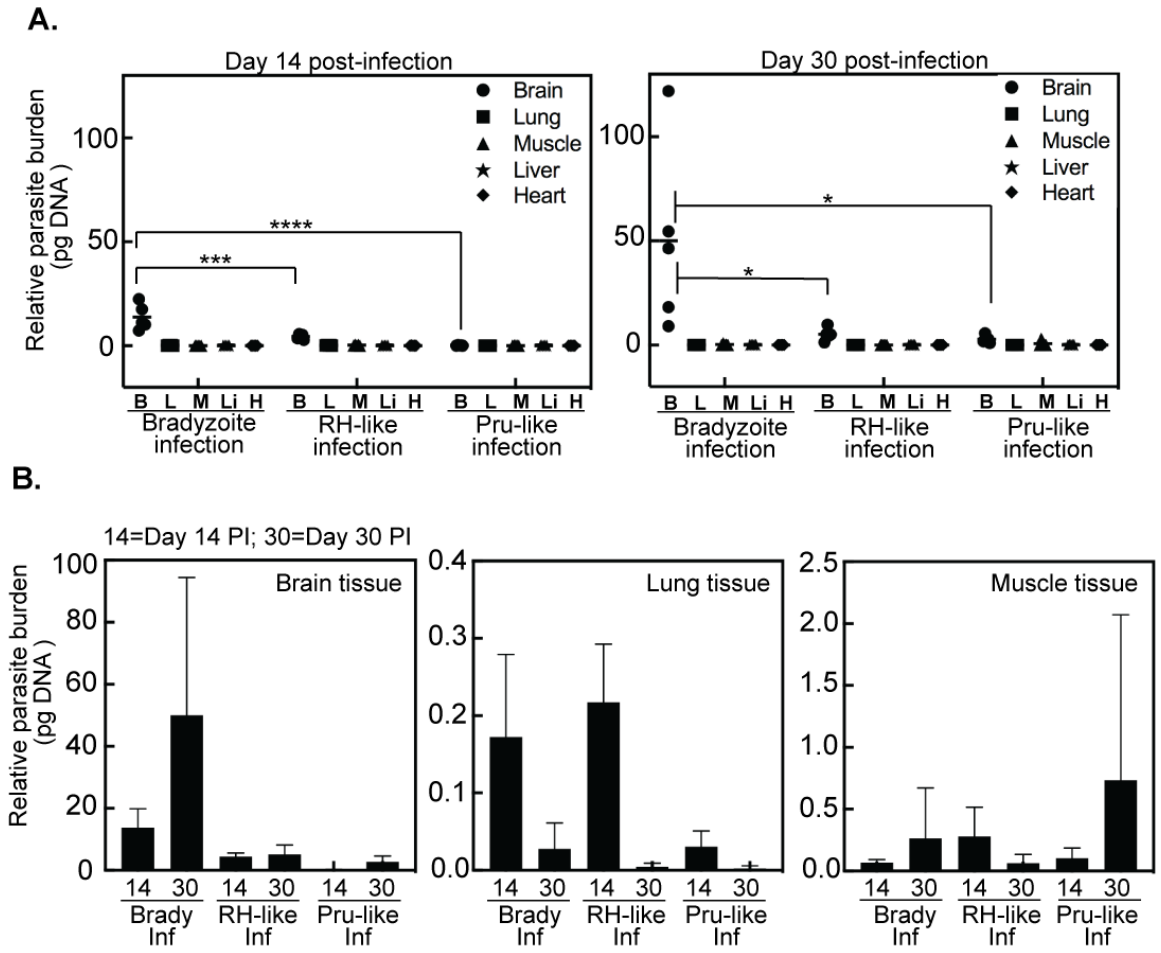

Figure 7. Parasite burden in mice infected with native bradyzoites, RH-like and Pru-like parasites. [A.] CBA/j mice were inoculated i.p. with 10,000 native bradyzoites, or RH-like (Day 3-populations) or Pru-like (Day 7-populations) parasites from HFF cell cultures. At day 14 and 30 post-infection the indicated tissues were harvested, total DNA was extracted and parasite burden was determined following amplification of the B1 gene compared against a standard curve. Statistical significance (****, $p<0.0001$; ***, $p<0.0001$; *, $p<0.05$) is indicated. **[B.]** Relative parasite burden in three organs are compared; brain, lung, and leg muscle.

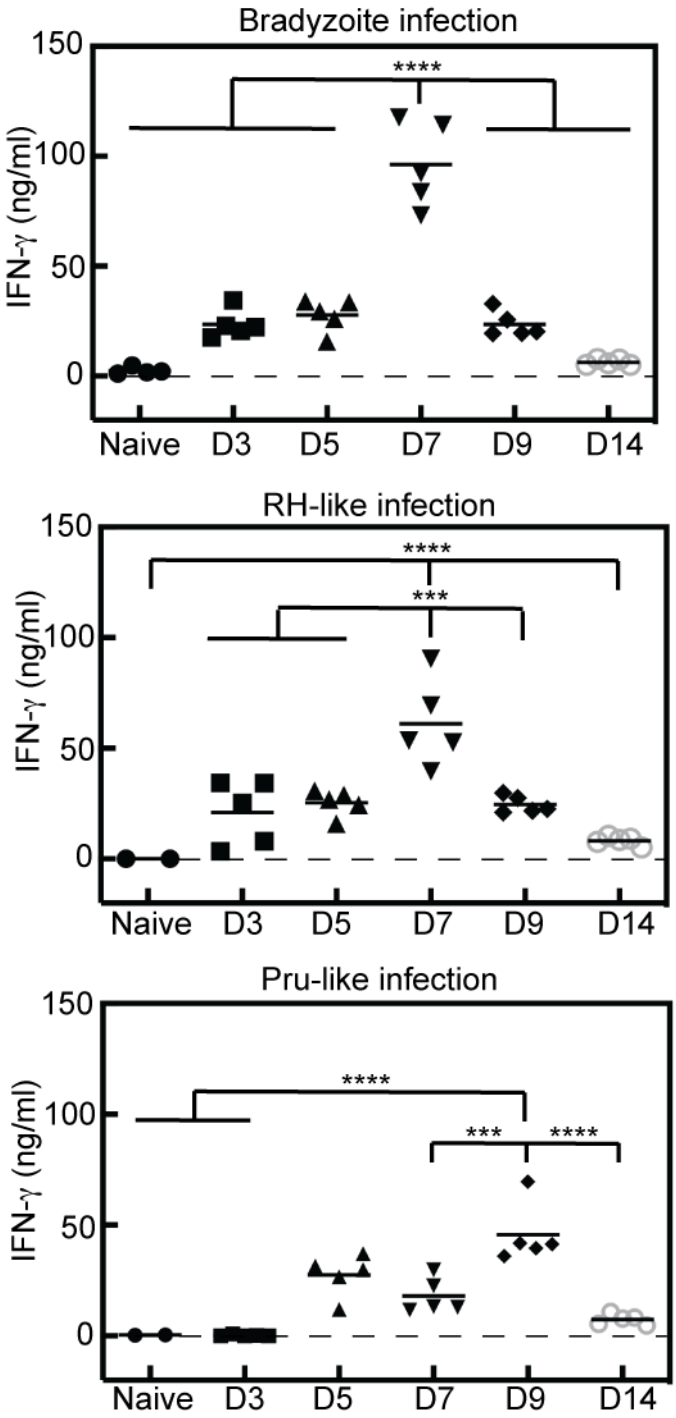

Figure 8. Cytokine analysis reveals differences in the levels and timing of IFNγ.
Serum was collected from infected animals from Figure 7 at days 3, 5, 7, 9, and 14 post-infection with native bradyzoites, RH-like or Pru-like parasites (derived from HFF cells), and systemic levels of IFNγ were quantified. Statistical significance (*, $p<0.05$; **, $p<0.001$) is indicated.

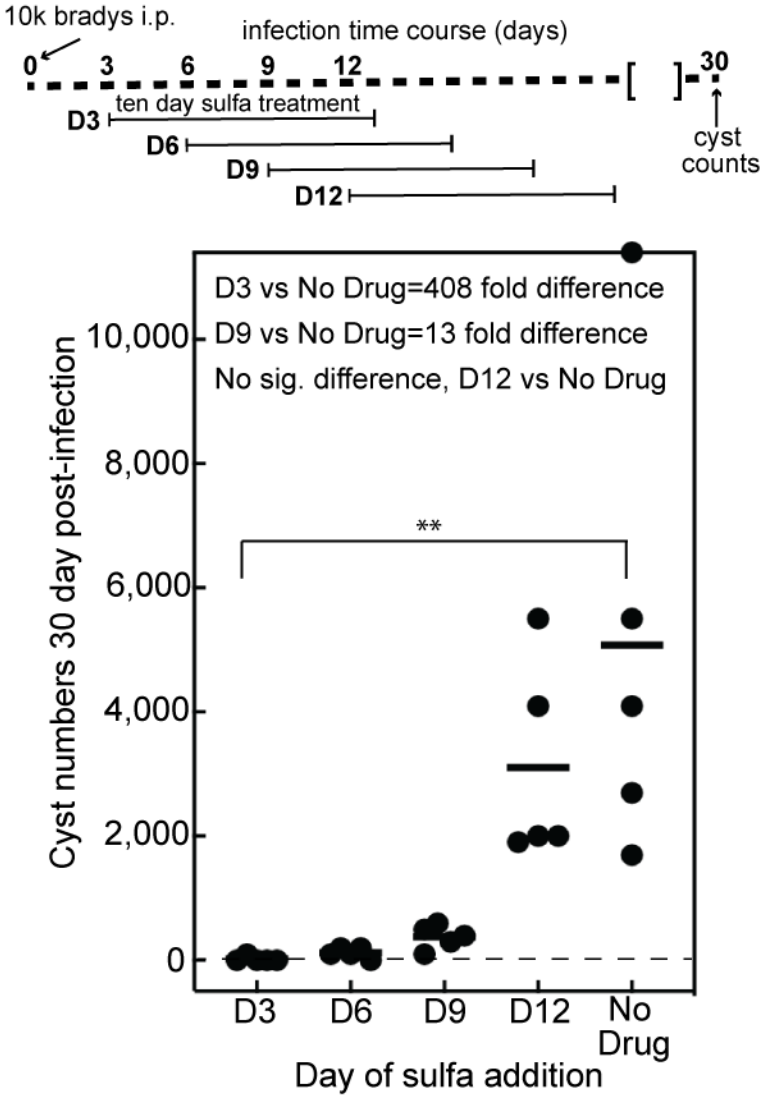

Figure 9. Early growth expansion of ME49EW parasites is critical for tissue cyst formation in mice.
Five groups of 5-CBA/j mice (25 total) were infected with 10k purified native ME49EW bradyzoites. The times of sulfamerazine (sulfa) addition and duration of treatment are indicated above the graph. Tissue cyst numbers per mouse brain were determined at 30 days post-infection. Statistical significance (**, $p<0.001$) is indicated. Note: The fold decrease in cyst number was >400 lower when the drug was added 3 h post-infection as compared to the no drug control and 13 fold lower when drug was added 9 days post-infection.